JOURNAL OF GEOPHYSICAL RESEARCH, VOL. 115, D01301, doi:10.1029/2009JD011973, 2010

An observational and modeling strategy to investigate the impact of remote sources on local air quality: A Houston, Texas, case study from the Second Texas Air Quality Study (TexAQS II)

W. W. McMillan,[1,2] R. B. Pierce,[3] L. C. Sparling,[1,2] G. Osterman,[4] K. McCann,[2] M. L. Fischer,[5] B. Rappenglück,[6] R. Newsom,[7] D. Turner,[8] C. Kittaka,[9,10] K. Evans,[2] S. Biraud,[5] B. Lefer,[6] A. Andrews,[11] and S. Oltmans[11]

Received 25 February 2009; revised 24 June 2009; accepted 9 September 2009; published 5 January 2010.

[1] Quantifying the impacts of remote sources on individual air quality exceedances remains a significant challenge for air quality forecasting. One goal of the 2006 Second Texas Air Quality Study (TexAQS II) was to assess the impact of distant sources on air quality in east Texas. From 23 to 30 August 2006, retrievals of tropospheric carbon monoxide (CO) from NASA's Atmospheric InfraRed Sounder (AIRS) reveal the transport of CO from fires in the United States Pacific Northwest to Houston, Texas. This transport occurred behind a cold front and contributed to the worst ozone exceedance period of the summer in the Houston area. We present supporting satellite observations from the NASA A-Train constellation of the vertical distribution of smoke aerosols and CO. Ground-based in situ CO measurements in Oklahoma and Texas track the CO plume as it moves south and indicate mixing of the aloft plume to the surface by turbulence in the nocturnal boundary layer and convection during the day. Ground-based aerosol speciation and lidar observations do not find appreciable smoke aerosol transport for this case. However, MODIS aerosol optical depths and model simulations indicate some smoke aerosols were transported from the Pacific Northwest through Texas to the Gulf of Mexico. Chemical transport and forward trajectory models confirm the three major observations: (1) the AIRS envisioned CO transport, (2) the satellite determined smoke plume height, and (3) the timing of the observed surface CO increases. Further, the forward trajectory simulations find two of the largest Pacific Northwest fires likely had the most significant impact.

Citation: McMillan, W. W., et al. (2010), An observational and modeling strategy to investigate the impact of remote sources on local air quality: A Houston, Texas, case study from the Second Texas Air Quality Study (TexAQS II), *J. Geophys. Res.*, *115*, D01301, doi:10.1029/2009JD011973.

1. Introduction

[2] Correctly attributing the relative impacts of remote sources on local air quality perhaps thousands of kilometers away remains a significant challenge for air quality forecasting. To achieve this, one requires local measurements, measurements in the source area, and measurements along the transport path. In addition, one must ascertain whether the prevailing meteorology allows transport paths between the suspected source and the observed air quality event. Modern satellite observations provide the large-scale view and in combination with transport models link the remote emissions to local observations. Here we present an integrated analysis of the impact of remote fires on Houston, Texas during a particular air quality exceedance event.

[3] Ranking fourth in national population, the Houston region also ranks fourth in severity of ozone pollution [*American Lung Association*, 2008]. In addition to a large sprawling population with its attendant vehicular traffic

[1]Department of Physics, University of Maryland Baltimore County, Baltimore, Maryland, USA.
[2]Joint Center for Earth Systems Technology, University of Maryland Baltimore County, Baltimore, Maryland, USA.
[3]Cooperative Institute for Meteorological Satellite Studies, STAR, NESDIS, NOAA, University of Wisconsin-Madison, Madison, Wisconsin, USA.
[4]Jet Propulsion Laboratory, California Institute of Technology, Pasadena, California, USA.
[5]Lawrence Berkeley National Laboratory, Berkeley, California, USA.
[6]Department of Earth and Atmospheric Sciences, University of Houston, Houston, Texas, USA.
[7]Pacific Northwest National Laboratory, Richland, Washington, USA.
[8]Space Science and Engineering Center, University of Wisconsin-Madison, Madison, Wisconsin, USA.
[9]NASA Langley Research Center, Hampton, Virginia, USA.
[10]Deceased 18 March 2009.
[11]Earth System Research Laboratory, NOAA, Boulder, Colorado, USA.

0148-0227/10/2009JD011973$09.00

emitting nitrogen oxides (NO_x), the Houston region is home to a large number of petrochemical industries releasing volatile organic compounds which combine to produce ozone as found during the first Texas Air Quality Study (TexAQS) study in 2000 [*Kleinman et al.*, 2002; *Ryerson et al.*, 2003; *Daum et al.*, 2004]. Similar to other geographic locations, meteorology plays a controlling role when ozone production is enhanced to levels exceeding the National Ambient Air Quality Standards (NAAQS) [*Kleinman et al.*, 2002; *Thompson et al.*, 2008; *Morris et al.*, 2010]. In particular, *Rappenglück et al.* [2008] found that northerly flow behind frontal passages and local sea breeze circulations often lead to large values of surface O_3 in Houston.

[4] During August and September 2006, the Texas Commission on Environmental Quality (TCEQ) sponsored an intensive operation period of TexAQS II as part of their development of a new State Implementation Plan (SIP) for attaining the NAAQS established by the United States Environmental Protection Agency (EPA). Identification of distant sources negatively influencing air quality in Texas and an impact assessment formed two key science questions targeted by TexAQS II. Recent tightening of the NAAQS for ground-level O_3 (EPA, National Ambient Air Quality Standards for ozone: Final rule, Federal Register, 73(60), 2008) has heightened the importance of this assessment. In particular, under the NAAQS Exceptional Events Rule, states can flag O_3 events if they can demonstrate extraordinary external sources caused the exceedance (EPA, The treatment of data influenced by exceptional events (exceptional event rule): Revised exceptional event data flagging submittal and documentation schedule to support initial area designations for the 2008 ozone NAAQS, *Federal Register*, 73(194), 2008). With this background, the State of Texas eagerly supported participation by NASA in TexAQS II to provide the large-scale satellite perspective of factors that affect air quality in Texas.

[5] Representatives from several NASA satellite instrument teams, including the Atmospheric InfraRed Sounder (AIRS) onboard the Aqua satellite and the Tropospheric Emission Spectrometer (TES) onboard the Aura satellite, were deployed in the field during TexAQS II to provide quick-look satellite data, interpretation for flight planning, and preparation of rapid synthesis reports. This paper stems from one such rapid synthesis report prepared by the two leading authors and a general science interest article in a NASA publication [*Naranjo*, 2008]. In the subsequent analyses, the satellite observations help to provide the large scale context for detailed surface and aircraft air quality measurements. As demonstrated here and by *Pierce et al.* [2009], the satellite observations assist with estimates of regional and continental scale distant source impacts on the background distribution of ozone and its precursors.

[6] As a direct atmospheric pollutant resulting from incomplete combustion and a precursor to the formation of tropospheric ozone (O_3), measurements of carbon monoxide (CO) are important to monitor and forecast air quality [*Crutzen et al.*, 1979; *Logan et al.*, 1981]. With a lifetime of two weeks to three months, tropospheric CO can be transported far downwind from its emission source [*Badr and Probert*, 1994]. Biomass burning represents the largest CO source with substantial interannual variations and demonstrated long-range impacts [*Forster et al.*, 2001; *Novelli et al.*, 2003; *Colarco et al.*, 2004; *Yurganov et al.*, 2008].

[7] Previous studies have utilized AIRS CO observations to illustrate the impact of long range transport on local air quality [*Stohl et al.*, 2007b, 2007a; *Thompson et al.*, 2007; *Zhang et al.*, 2008; *McMillan et al.*, 2008b] and the impact of distant fires on air quality in the vicinity of Houston, Texas [*Morris et al.*, 2006]. However, all these studies involved tracking CO transport in the midtroposphere with much of the long-range transport occurring between 400 and 600 mb [*McMillan et al.*, 2008b]. In the present case, we examine transport of CO emissions from fires in the United States Pacific Northwest and subsequent transport of CO occurring between 700 mb and the surface, a more difficult atmospheric region for satellite instruments, particularly AIRS, to probe. Quantifying the impact of these fires on Houston air quality will require detailed modeling of the timing, amount, and altitude of injection of the fire emissions. Employing satellite observations to quantify and apportion causes of individual air quality exceedances remain a significant challenge for the assessment community. Here, we present a suite of observations for one case illustrating the complexity of these challenges. In section 2, we summarize the various observational and model data sets examined and the integrated strategy employed in this study. In section 3, we detail the analyses of each data set and integrate the findings to illustrate the impact of the Pacific Northwest fires on Houston's air quality during this event.

2. Data and Methodology

[8] This study integrates observations from four satellite instruments and five surface sites (with multiple instruments and some profiles) in conjunction with trajectory simulations and a chemical transport model. Table 1 summarizes these observational and model data sets with the principle findings of each and relevant references for the instrument or technique. The different data sets are listed in their order of description in this section and discussion in section 3. The numbers leading each entry in Table 1 are used in the following instrument and data description. The strategy (flow) of the analysis follows by reading straight down the Principle Findings column.

[9] O_3 surface observations (data set 1 in Table 1) were made at the Clear Lake EPA AIRnow site 48201572, also TCEQ site 572, in suburban Houston (Texas Commission on Environmental Quality, http://www.tceq.state.tx.us/cgi-bin/compliance/monops/site_photo.pl?cam%s=572, 2009; hereafter TCEQ, online report, 2009) (also EPA, http://airnow.gov/, 2006; hereafter EPA, online report, 2006). This instrument is part of the EPA State and Local Air Monitoring Stations (SLAMS) and is a regulatory quality instrument. Back trajectories (data set 2) for this site were computed with the Real-time Air Quality Modeling System (RAQMS) model [*Pierce et al.*, 2007] using six hour forecasts (University of Wisconsin-Hybrid dynamical core) initialized with the full spectral resolution Global Forecast System (GFS) National Center for Environmental Prediction (NCEP) analyses [*Pierce et al.*, 2009]. Ozonesondes (data set 3) were launched from the University of Houston as part of the Ozone Network Study, 2006 (IONS-06)[*Thompson et al.*, 2008; *Morris et al.*, 2010].

Table 1. Summary of Observational and Model Data Sets and Their Principle Findings

Data Set	Platform	Instrument or Location	Observation or Retrieval	Principle Findings	Method References
1	surface	Houston, TX (Clear Lake)	O_3	observed air quality exceedance	TCEQ (online report, 2009) EPA (online report, 2006)
2	model	RAQMS	back trajectories	documents frontal passage in Houston with O_3 increase	*Pierce et al.* [2009]
3	profiles	ozonesondes U. Houston	O_3, T(p), winds	observed O_3 increase over Houston	*Morris et al.* [2010] *Thompson et al.* [2008]
4	Aqua satellite	AIRS	CO	observed CO transport from NW fires to Houston	*McMillan et al.* [2008b, 2008a]
5	Aqua satellite	MODIS	hot spots, AOD	observed NW fire locations, little smoke transport to Houston but aerosol arc over Gulf of Mexico	*Giglio et al.* [2003], *Schroeder et al.* [2008] *Kaufman et al.* [1997], *Chu et al.* [2003] *Remer et al.* [2005], *Levy et al.* [2007]
6	CALIPSO satellite	CALIOP	aerosol profiles	observed smoke profile downwind of fires	*Winker et al.* [2007] *Labonne et al.* [2007], *Kahn et al.* [2008]
7	Aura satellite	TES	CO	observed lower tropospheric CO in transport to Houston	*Luo et al.* [2007]
8	surface	Lamont, OK (SGP site)	CO	observed CO plume mix-down in transit to Houston	*Fischer et al.* [2007]
9	profiles	Lamont, OK (SGP site)	lidar aerosol profiles	did not observe smoke with CO plume	*Goldsmith et al.* [1998] *Turner et al.* [2002]
10	surface	Moody, TX (KWKT tower)	CO, O_3	observed CO plume mix-down in transit to Houston	*Zhao et al.* [1997], *Bakwin et al.* [1998] *Andrews et al.* [2008, also online report, 2008]
11	surface	Houston, TX (U. Houston)	CO, O_3	observed CO plume mix-down in Houston	Lefer and Rappenglück (submitted manuscript, 2009) *Rappenglück et al.* [2008]
12	surface	Houston, TX (Deer Park)	speciated aerosols	observed organic carbon increase with CO in Houston	EPA (online report, 2008)
13	model	GKFTC	forward trajectories	tracks NW fire emissions to Houston and produces arc over Gulf of Mexico	*Schoeberl and Sparling* [1995]
14	model	RAQMS	CO, carbon aerosols	tracks CO and carbon aerosol transport from NW fires to Houston and Gulf	*Pierce et al.* [2007, 2009]

[10] All AIRS CO data (data set 4) presented herein utilize version 5.0.14.0 (v5) Level 2 AIRS standard products archived at the NASA Goddard Earth Sciences Data and Information Services Center (GES DISC). These AIRS CO retrievals were screened for the highest quality following the guidelines in AIRS Level 2 data documentation [*AIRS Project Office*, 2007a, 2007b] where the quality flag, Qual_CO, equals zero. This quality control criterion assesses the quality of AIRS midtropospheric temperature retrievals [*Susskind et al.*, 2010], cloud fractions <90%, and degrees of freedom in the CO retrievals >0.5.

[11] Tropospheric aerosol optical depth (AOD) retrievals (data set 5) from the MODerate resolution Imaging Spectroradiometer (MODIS) MYD04 collection 005 Level 2 were downloaded from the Level 2 and Atmosphere Archive and Distribution System (LAADS). The depicted values are AOD at 550 nm as found in the Optical_Depth_Land_And_Ocean variable in the Level 2 files [*Kaufman et al.*, 1997; *Chu et al.*, 2003; *Remer et al.*, 2005; *Levy et al.*, 2007]. Aerosol profile data (data set 6) from the Cloud-Aerosol Lidar with Orthogonal Polarization (CALIOP) instrument onboard the Cloud-Aerosol Lidar and Infrared Pathfinder Satellite Observation (CALIPSO) satellite were obtained through the CALIPSO Science Team. TES data (data set 7) version 3 was provided through the TES Science Team.

[12] Continuous CO measurements (data set 8) were collected at 60 m above ground level at the United States Department of Energy Atmospheric Radiation Measurement (ARM) Climate Research Facility in the Southern Great Plains (SGP) near Lamont, Oklahoma, 36.61°N, 97.49°W. The SGP CO measurements were acquired with a nondispersive infrared gas correlation instrument (Thermo Scientific TE-48C) modified with additional pressure control, frequent zero correction, and multipoint calibrations to provide precision and accuracy near 5 ppbv as judged by comparison with NOAA network flask measurements. For additional details, see the previous research of *Potosnak et al.* [1999] and A. Andrews et al. (Carbon dioxide and carbon monoxide dry air mole fractions from the NOAA ESRL Tall Tower Network, 1992–2008, Version: 2008-10-02, 2008, available at ftp://ftp.cmdl.noaa.gov/ccg/towers/) (hereinafter Andrews et al., online report, 2008). Sensible heat flux, wind speed, and wind direction were also measured at 60 m with equipment similar to that previously used by *Fischer et al.* [2007] on a 4 m tower. Aerosol profiles (data set 9) were made at this site by a Raman Lidar [*Goldsmith et al.*, 1998; *Turner et al.*, 2002].

[13] Nearly 600 km due south of the SGP site, additional ground-based measurements were made at the KWKT TV tower (data set 10) in Moody, Texas, 31.32°N, 97.33°W, instrumented by NOAA Earth System Research Laboratory for measurements of CO, CO_2, O3, and meteorology as part of their tall tower program [*Zhao et al.*, 1997; *Bakwin et al.*, 1998; Andrews et al., online report, 2008].

[14] Roughly 260 km southeast of the KWKT tower, high quality CO, O_3, and meteorological measurements were obtained on the roof of the Moody Tower dormitory (data set 11) at the University of Houston, 29.72°N, 95.34°W (B. Lefer and B. Rappenglück, The TexAQS-II Radical and Aerosol Measurement Project (TRAMP), submitted to *Atmospheric Environment*, 2009; B. Lefer et al., Photochemical and meteorological relationships during the TexAQS-II

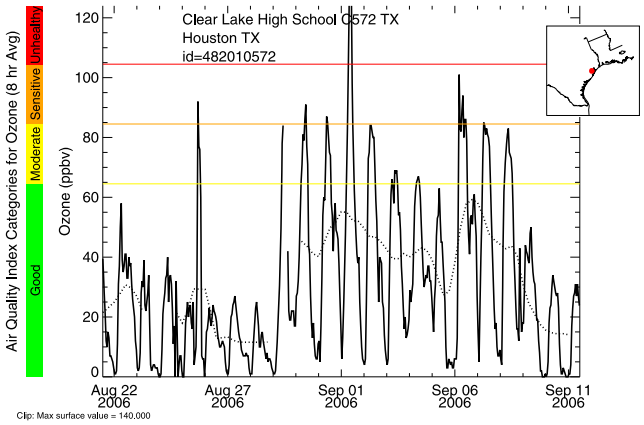

Figure 1. Time series of surface ozone mixing ratio at the Clear Lake EPA AIRNow site in Houston, Texas. The dotted line represents a 24 hour running mean of 6 hourly observations.

Radical and Aerosol Measurement Project (TRAMP), submitted to *Atmospheric Environment*, 2009). EPA speciated aerosol measurements at several sites in Texas (data set 12), and the Deer Park site (ID 482011039), 29.67°N, 95.13°W, in suburban Houston in particular, were also used (EPA, Air Quality System, http://www.epa.gov/ttn/airs/airsaqs/, 2008; hereafter EPA, online report, 2008).

[15] Forward trajectory simulations (data set 13) were performed with the Goddard Kinematic Forward Trajectory Code (GKFTC) [*Schoeberl and Sparling*, 1995] using both Global Forecast Model (GFS) and NCEP reanalysis winds. CO and carbonaceous aerosol output fields (data set 14) from the RAQMS model were used in addition to the previously mentioned back trajectories (data set 2). In RAQMS, an emissions database specifies anthropogenic sources and MODIS hot spot, fire severity, and ecosystem based fuel loading are used to partition biomass burning emissions [*Pierce et al.*, 2007]. The RAQMS $2° \times 2°$ CO and black carbon and organic carbon aerosols (BCOC) analysis includes assimilation of TES CO retrievals [*Pierce et al.*, 2009] and MODIS aerosol optical depth [*Sunita et al.*, 2009] and therefore provides a quantitative although coarse depiction of the synoptic scale distribution of CO and BCOC over the continental United States.

3. Detailed Analysis and Interpretation

[16] Following the strategy outlined in the principle findings column of Table 1, we commence the detailed analysis and interpretation with observations of the O_3 air quality exceedance in Houston and the change in air mass due to the passage of a cold front. Thereafter, we discuss the satellite observations starting with AIRS and MODIS, CALIPSO, and TES. Next, we investigate the CO and O_3 observations from surface sites which document southward passage of the CO plume along the transport path from the Pacific Northwest fires to Houston with mixing to the surface. Finally, a combination of simulations from GKFTC and RAQMS confirm the three major findings: (1) the AIRS envisioned CO transport, (2) the CALIPSO determined smoke plume height, and (3) the timing of the surface CO increases. The GKFTC simulations indicate emissions from the Pueblo Fire in southeastern Oregon produced the MODIS observed aerosol arc over the northern Gulf of Mexico. RAQMS also predicts carbonaceous aerosol transport from the fires to the Gulf of Mexico.

3.1. Houston Air Quality Exceedance

[17] From August 31 through September 4, 2006, Houston, Texas, experienced the worst ozone exceedance of the summer [*Pierce et al.*, 2009; *Rappenglück et al.*, 2008; *Morris et al.*, 2010]. The peak of this event occurred on different days at different EPA AIRNow sites throughout the Houston metropolitan statistical area (MSA). Figure 1 presents the time series of surface ozone concentrations from the Clear Lake EPA AIRNow site in Houston, Texas, where the daily maximum in surface O_3 began increasing on 29 August with an overall peak on 1 September.

[18] This time period occurred after the passage of a cold front on 29 August 2006 and an associated change in lower tropospheric wind direction from the south/southeast to the north as indicted by the change in surface layer back trajectory paths shown in Figure 2. Additional meteorological details are given by *Rappenglück et al.* [2008] and Lefer and Rappenglück (submitted manuscript, 2009). Previous researchers have found the largest values of surface O_3 and CO in the Houston area occur typically during conditions of northerly flow [*Rappenglück et al.*, 2008; Lefer et al., submitted manuscript, 2009] and often are associated with a strong local sea breeze circulation [*Davis et al.*, 1998; *Darby*, 2005; *Rappenglück et al.*, 2008]. The sea breeze circulation serves both to recycle local pollutants in the Houston MSA and to provide regions of localized convergence on shore [*Rappenglück et al.*, 2008]. *Pierce et al.* [2009] have associated a portion of the 1–4 September 2006 O_3 increase to the import of enhanced background O_3 with influence from the industrial upper Midwest and Great Lakes regions particularly through the impact of NO_x on O_3 production. This enhanced background influence on Houston O_3 continued until 8 September as reflected in the Clear Lake O_3 time series of moderate O_3 conditions from 29 August to 8 September [*Pierce et al.*, 2009] during northerly flow and the combined sources in the Great Lakes region and the Pacific Northwest fires.

[19] Figure 3 indicates an increasing O_3 concentration as the 1 September RAQMS surface trajectories approach Houston while remaining in the boundary layer. However, note the proximity of the trajectories to the nocturnal boundary layer on the three nights prior to arrival in Houston. Although the RAQMS surface trajectories seem to remain in the boundary layer where there are numerous sources of O_3 precursors, the paths of the trajectories in Figure 2 largely avoid major population and industrial areas to the north. In contrast, *Pierce et al.* [2009, Figure 5] found the 2 September surface trajectories tap NO_x rich populated and industrial areas around Lake Michigan.

[20] This O_3 episode in the Houston area was well documented by a number of ozonesondes flown as part of IONS-06 [*Thompson et al.*, 2008; *Morris et al.*, 2010]. Figure 5b of *Thompson et al.* [2008] illustrates that not only did the near surface and boundary layer O_3 increase following the cold frontal passage on 29 August but O_3 abundances throughout the lowest 6 km increased. Between 2 and 3 km, O_3 increased from 30 ppbv on 28 August to

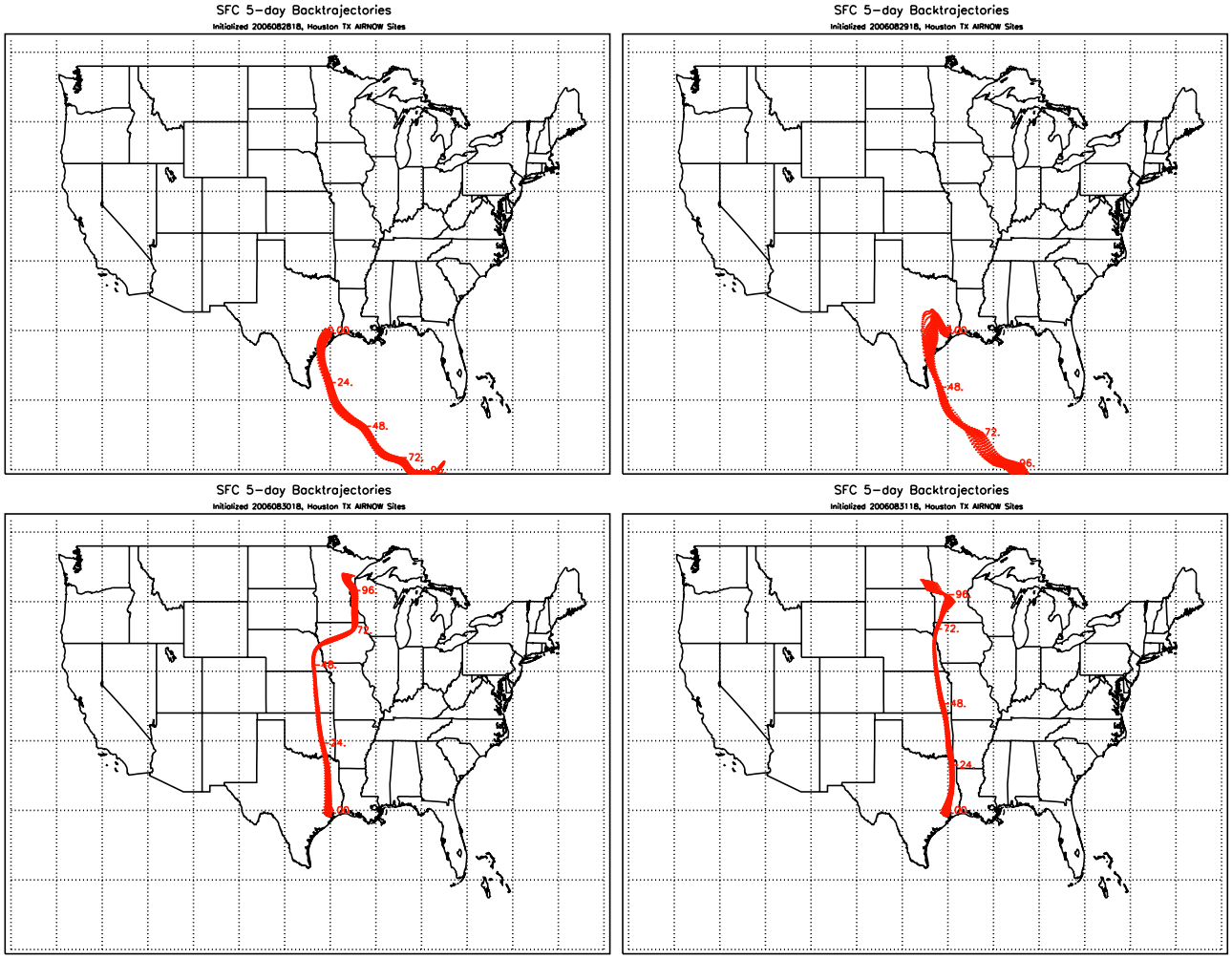

Figure 2. Four day sequence of five day back trajectories from the Houston MSA EPA AIRNow sites initialized at the surface at 1800 UTC: (top left) 28 and (top right) 29 August and (bottom left) 30 and (bottom right) 31 August. The passage of a cold front on 29 August is evident in the change in trajectory paths from southerly to northerly.

50–60 ppbv on 30 August. The timing of this increase is consistent with transport from the 23 August Pacific Northwest fires as detailed in the following subsections describing AIRS CO and forward trajectory simulations. Layers of larger O_3 enhancements are evident in the 1200 UTC ozonesondes of 31 August and 1 September. Back trajectories computed for these layers indicate the 28 August Pacific Northwest fires as possible sources with little mixing of this material to the surface near Houston (G. Morris, personal communication, 2008).

3.2. Satellite Observations

[21] Similar to AIRS Science Team support for NASA's INTEX-A field experiment [*McMillan et al.*, 2008b], during TexAQS II, near-real-time (NRT) AIRS retrieval products were generated at the University of Maryland, Baltimore County from NRT AIRS spectra provided by NOAA National Environmental Satellite, Data, and Information Service (NESDIS) and the GES DISC using the NOAA research version of the AIRS Team retrieval algorithm. We first present the AIRS CO observations similar to those examined in the field. Following this, we present observa-

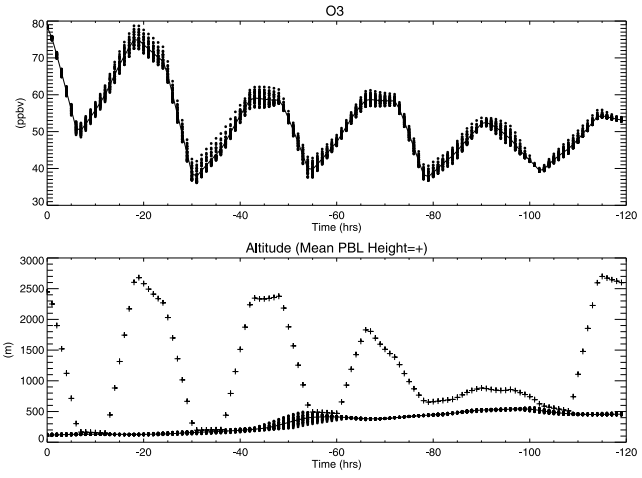

Figure 3. (top) Five day Lagrangian mean ozone mixing ratio along the RAQMS back trajectories from the Houston MSA AIRNow sites initialized at the surface at 1800 UTC on 1 September 2006. (bottom) Altitude of these trajectories and the PBL height along the trajectories (pluses).

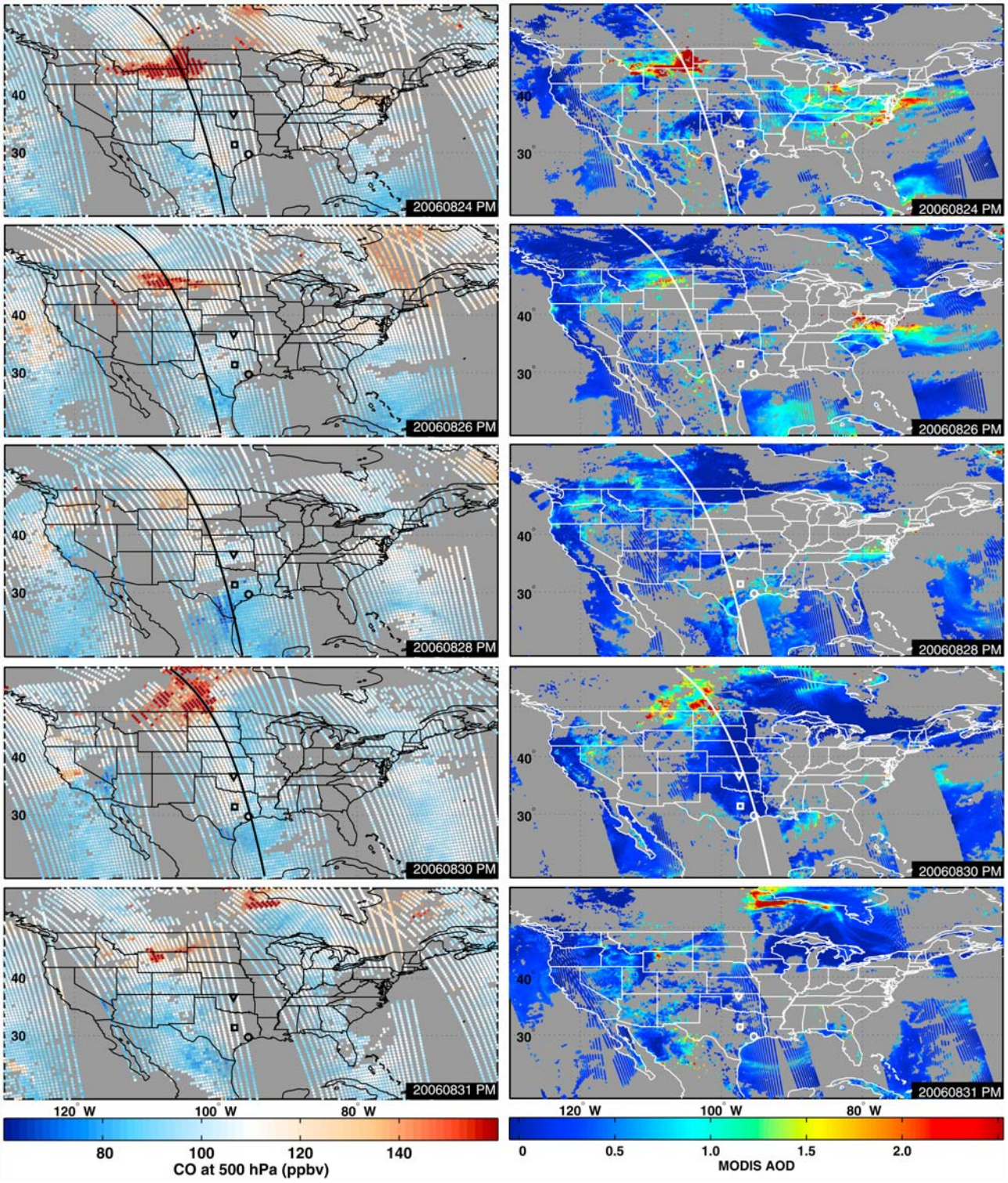

Figure 4. Maps of (left) AIRS 700 mb CO and (right) Aqua MODIS AOD from the afternoon orbits of 24, 26, 28, 30, and 31 August 2006 over the continental United States. The location of a CALIPSO cross section is indicated by the heavy black (white) line arcing through the central United States on the 24 August maps, and similarly for TES cross sections on 26, 28, and 30 August maps. Locations of the ARM SGP site (triangle), WKT tower (square), and Houston (circle) are noted for reference.

tions from MODIS onboard Aqua, the CALIPSO lidar, and TES onboard Aura to support our analysis of the AIRS observations and to provide crucial information on the vertical distribution of the observed CO.

3.2.1. AIRS CO and MODIS AOD

[22] Figure 4 presents maps of AIRS 700 mb CO (left) and Aqua MODIS AOD (right) for the afternoon orbits (nadir ~1330 local time) of 24, 26, 28, 30, 31 August 2006 over

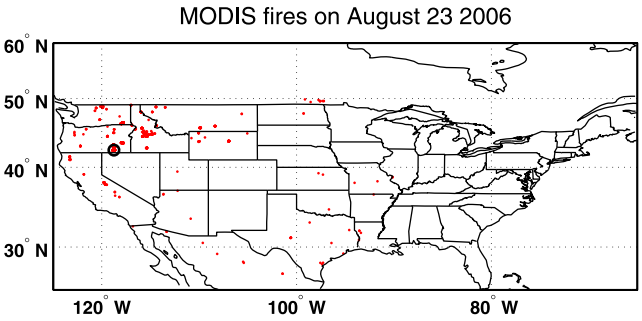

Figure 5. Locations of MODIS detected hot spots on 23 August 2006 over the western United States. All hot spots detected by the Terra and Aqua MODIS during both daytime and nighttime orbits are shown. The location of the Pueblo Fire in southeastern Oregon is noted by the black circle.

the continental United States. As discussed in more detail in sections 3.2.3, 3.3, and 3.4, for this case it appears much of the CO AIRS sees transported across the central United States resides at or below 700 mb. Thus, here we present maps of AIRS CO retrievals at 700 mb. Version 4 AIRS CO retrievals have been validated as accurate to within 15% at 500 mb [*McMillan et al.*, 2008b]. Ongoing validation of AIRS v5 CO retrievals indicates accuracy from 300 to 900 mb to 10% with an RMS <10% [*McMillan et al.*, 2008a]. This does not mean multiple pieces of vertical information can be retrieved from AIRS spectra. Typically, the degrees of freedom in the v5 CO retrieval is near one (typically larger in the daytime and in regions of enhanced CO concentration) indicating AIRS is most sensitive to the total column. However, the shape of the averaging kernels varies from retrieval to retrieval giving some indication of where CO enhancements lie in the vertical.

[23] The 24 August maps demonstrate excellent spatial correlation between the large CO abundances and AOD stretching from central Idaho, along the southern border of Montana into the Dakotas, and north into Canada. This CO rich smoke plume emanated from a number of large fires where activity peaked on 23 August with more than 1100 MODIS detected hot spots across the Pacific Northwest and Northern Plains (40° to 50°N, 125° to 90°W) as set forth in Figure 5. Figure 6 indicates fire activity peaked across the entire western United States (west of 90°W) on 23 August and was most concentrated in the northwestern United States. In particular, the largest concentration of fire activity from 22 to 24 August was in north central Washington (the Tripod Complex Fire), southeastern Washington (the Columbia Complex Fire, 46.1°N to 46.4°N, 118.1°W to 117°W), eastern and southeastern Oregon (the South End Complex Fires including the Pueblo Fire, 42.2°N to 42.5°N, 119°W to 118.5°W), and central Idaho. The location of the Pueblo Fire is noted in Figure 5.

[24] The South End and Columbia Complex Fires were sparked by dry lightning from thunderstorms associated with a cold front as it moved across the region on 21 August. The South End Complex Fire blackened more than 117,000 acres in the Steens Mountains between 21 and 24 August with the Pueblo Fire the largest at 78,000 acres. The Columbia Complex Fire scorched 79,000 acres by 1 September and an additional 38,000 acres by 13 September. The Tripod Complex Fire started in early August with 62,000 of its total 142,000 acres burning between 14 and 29 August.

[25] By 26 August, the majority of the CO plume moved across Canada with a portion remaining over the Northern Plains and stretching across eastern Montana and the Dakotas to southern Minnesota. This is the vicinity of the ending points of the 5 day back trajectories from the Houston MSA AIRNow sites from 31 August depicted in Figure 2. Note the MODIS AOD associated with the CO plume appears to be dissipating faster than the CO.

[26] The MODIS AOD over the Northern Plans continues to wane as AIRS shows substantial CO remaining over eastern Montana on 28 August and moving south into Kansas and the Texas Panhandle. Despite the smaller footprint of the MODIS AOD retrievals versus the AIRS CO retrievals, many of the MODIS AOD retrievals across the central United States appear cloud contaminated on 26 and 28 August. This lack of AOD retrievals complicates the direct tracking of the smoke plume. AIRS cloud-clearing techniques [*Susskind et al.*, 2003] enable CO retrievals for scenes up to 90% cloudy.

[27] By 30 August, an elongated region of enhanced CO stretches south from western North Dakota to near the Texas Gulf coast while MODIS AOD displays only a faint north-northwest/south-southeast trend of AOD ~0.5 to the west of the TES track and some higher values in southern and eastern Texas (Figure 4). Far from the most obvious feature in the CO maps, this is only a 20 ppbv (~20%) CO enhancement when compared to areas to the east and west. CO and smoke emissions from the 28–30 August fires in the Pacific Northwest move toward both the northeast into Canada and the southwest across central California as evident in both the AIRS and MODIS maps.

[28] The 31 August MODIS AOD map shows an arcuate aerosol feature stretching across the northern central Gulf of Mexico. Unfortunately, the location of this arc falls in a gap

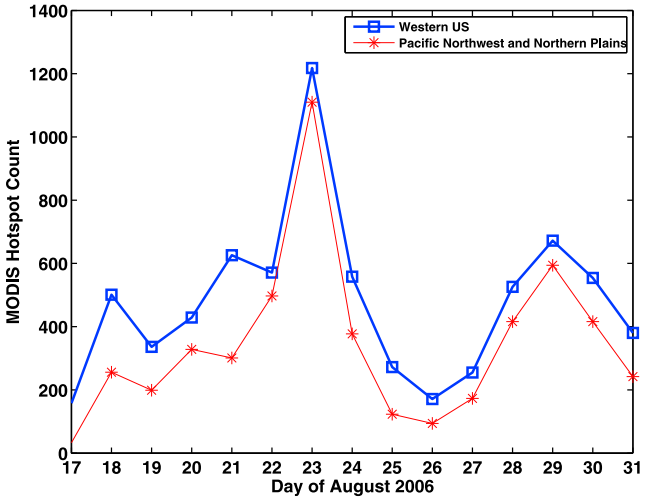

Figure 6. Time series of all MODIS detected hot spot counts across the entire western United States (blue squares) and in the northwestern United States (red asterisks).

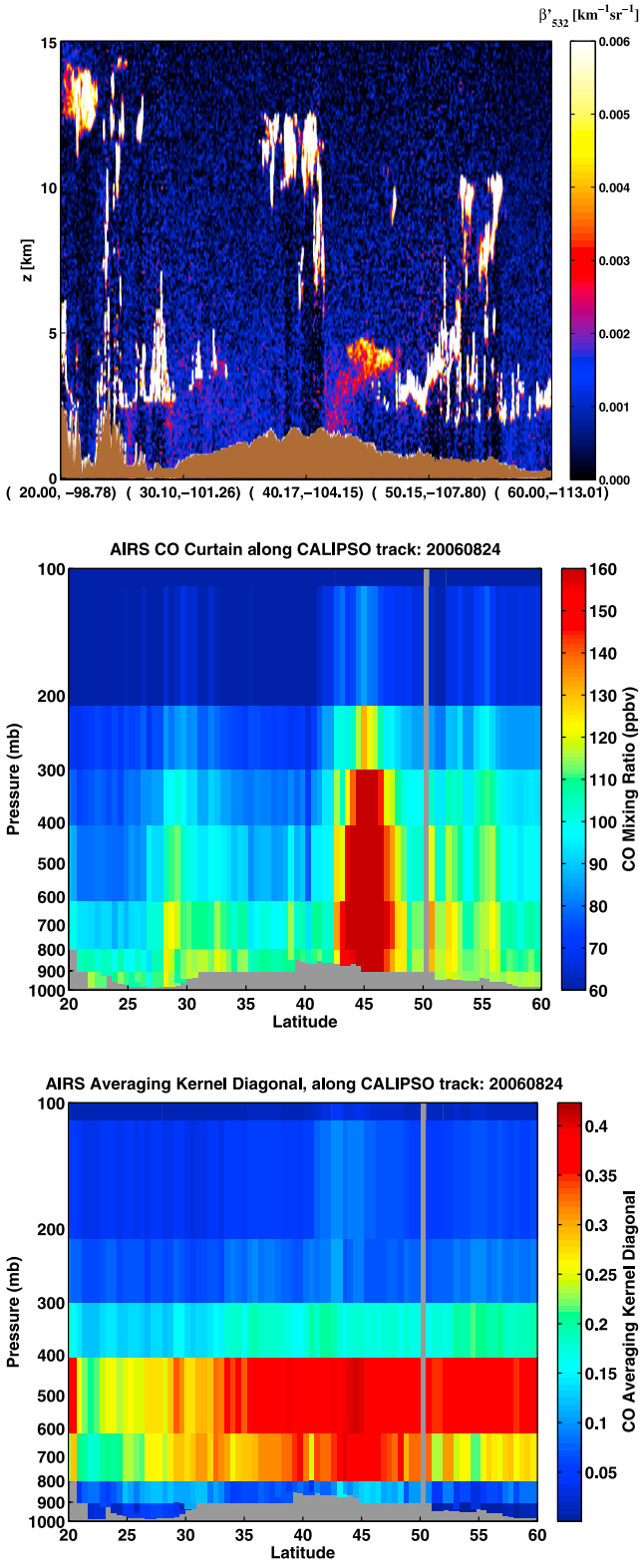

Figure 7. (top) CALIPSO attenuated backscatter coefficient cross section along the track illustrated in the 24 August AIRS CO and MODIS AOD maps (Figure 4). (middle) Retrieved AIRS CO cross section along this same track. (bottom) Cross section of the diagonal of the AIRS CO averaging kernels.

between orbits for AIRS CO data on this date (Figure 4), and no corresponding CO arc is evident. Forward trajectory simulations presented in a following subsection find this aerosol arc closely resembles a portion of the 23 August emissions from the Pueblo Fire in southeastern Oregon. The location of this arc closely follows the position of the cold front on this day (see Figure 2 of Lefer et al., submitted manuscript, 2009).

[29] Although some of the smoke from the Pacific Northwest wildfires must have crossed through Houston to form the arc over the Gulf of Mexico, much of the smoke aerosols could have been scavenged by the extensive clouds seen by both MODIS and AIRS. Due to the lack of a discernable MODIS aerosol feature throughout the transport event, we were unable to perform a detailed correlation study with AIRS CO to look for changes in plume height as was accomplished by *McMillan et al.* [2008b] for the smoke plume from Alaskan fires in 2004. Additional details of these maps, the inferred transport, pertinent satellite observations, and trajectory and chemical transport model simulations are discussed in section 3.3.

3.2.2. CALIPSO and AIRS Cross Sections

[30] Because both AIRS CO and MODIS AOD retrievals lack the vertical sensitivity to specify uniquely the vertical extent of the smoke plume, we examined the aerosol cross sections from the CALIOP lidar onboard the CALIPSO satellite [*Winker et al.*, 2007] now following less than two minutes behind AIRS onboard Aqua in orbit. CALIPSO data has been used previously to determine the injection height of smoke aerosols [*Labonne et al.*, 2007; *Kahn et al.*, 2008].

[31] As luck would have it, of all the daytime CALIPSO orbital tracks between 23 August and 1 September, only the track of 24 August was sufficiently cloud free to unambiguously identify the target smoke plume. However, this one cross section is key to pinning the altitude of the smoke plume just one day downwind of the fires burning in Washington, Oregon, and Idaho. We discuss this further in the Trajectory and Model Simulation subsection to follow. Several of the nighttime CALIPSO tracks saw portions of this plume, but clouds obscured the view as the plume moved south into the central plains.

[32] The AIRS CO and MODIS AOD maps for 24 August (Figure 4) show the location of the afternoon 24 August CALIPSO cross section as it slices through the CO rich smoke plume across northeastern Wyoming and southeastern Montana. The smoke plume is readily evident in Figure 7 (top) as the red to orange feature ascending from the surface near 42°N and flaring towards 48°N with a top just below 5 km. Figure 7 presents the CALIPSO 532 nm total attenuated aerosol backscatter, β, averaging 15 profiles (approximately 5 km) along its track. For this daytime orbit, the depolarization ratio is very noisy, but the color ratio for the smoke plume is substantially different from the surrounding clouds. The standard vertical feature mask denotes this as an aerosol feature.

[33] Figure 7 (middle) demonstrates the spatial coincidence of the CO feature in the 24 August CO map (Figure 4). Although the AIRS retrieval lacks the sensitivity to resolve the vertical structure apparent in the CALIPSO aerosols, the diagonal of the averaging kernel shown in Figure 7 (bottom) indicates the CO enhancement peaks between 400

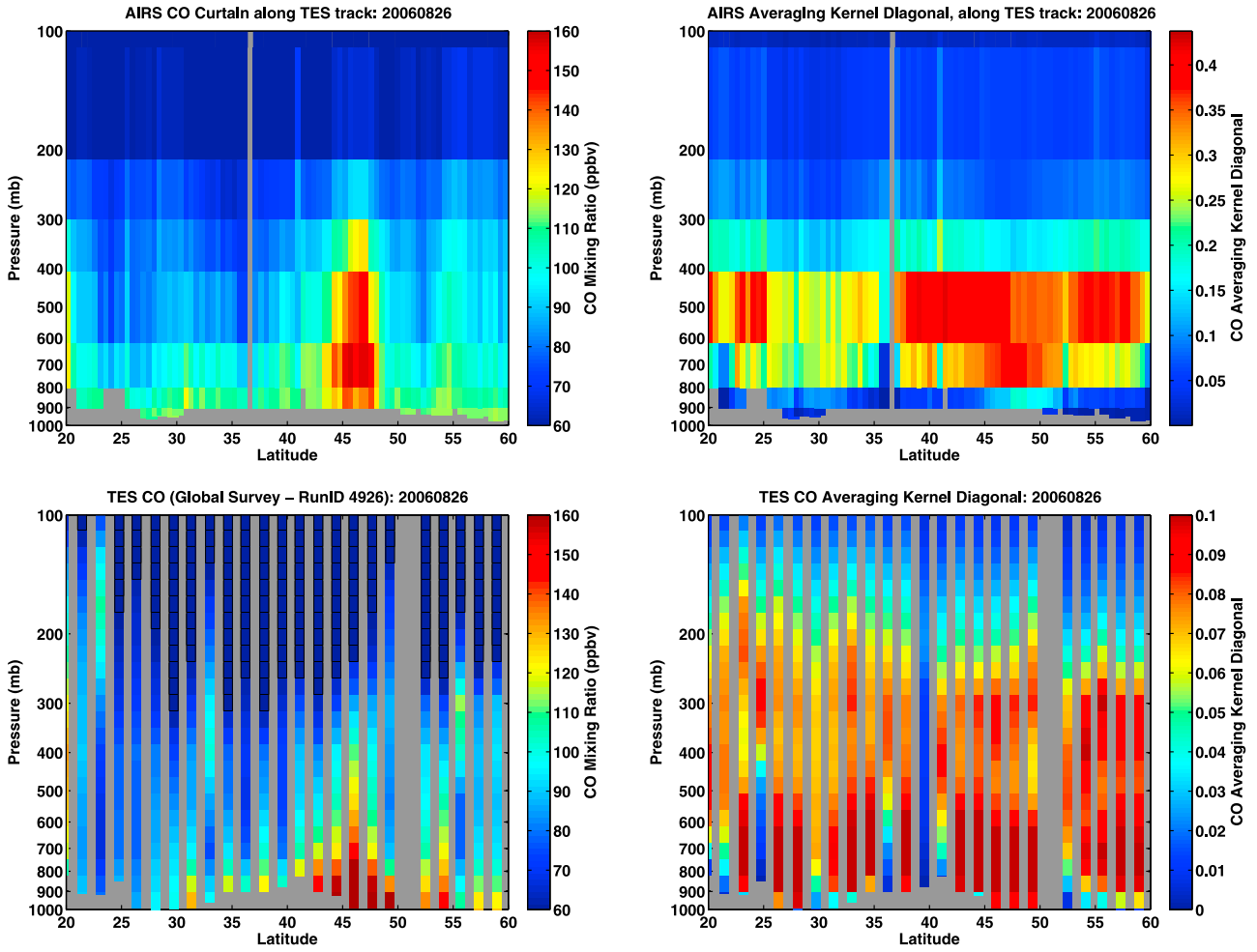

Figure 8. The 26 August global survey track: (top) AIRS and (bottom) TES cross sections of (left) retrieved CO and (right) diagonal of the CO averaging kernel. The location of these cross sections is noted in the AIRS CO and MODIS AOD maps of Figure 4.

and 600 mb (4–6.5km). Further, in the region of the CO enhancement between 42°N and 50°N, the magnitude of the diagonal of the averaging kernel in the 800–900 mb region is twice as large as in areas to the north and south. As discussed more in the next section with plots of the full averaging kernels and comparisons to TES retrievals, this implies an enhanced sensitivity to the layers closest to the surface. This inferred altitude distribution for CO is consistent with the CALIPSO smoke plume.

3.2.3. TES and AIRS CO Cross Sections

[34] TES was designed to provide tropospheric profile retrievals of trace gases important to studies of air quality including CO and O_3 [*Beer*, 2006]. Validation of TES CO retrievals indicate they are accurate in the midtroposphere to approximately 10% [*Luo et al.*, 2007].

[35] AIRS and TES retrieved CO and diagonal of the averaging kernel cross sections for afternoon orbits over the central United States on 26, 28, and 30 August appear in Figures 8, 9, and 10, respectively. The locations of these observations are indicated in the AIRS CO and MODIS AOD maps of Figure 4. The TES data are from global survey measurements. The diagonals of the averaging kernels illustrate the different vertical sensitivities of the two instruments; AIRS generally peaks around 500 mb, and TES often peaks closer to the surface. The spatial agreement of CO features is excellent between the two instruments indicating they are observing the same phenomena. Unfortunately, TES performed no observations over the central United States during the afternoon orbits of 24 August; thus, no three way comparison between AIRS, TES, and CALIPSO is possible for this day.

[36] Figure 8 shows both instruments see the CO plume confined mainly below 600 mb over Montana on 26 August. By 28 August, both instruments continue to show CO closer to the surface between 45° and 50°N, and to the south over Kansas between 34° and 40°N (Figure 9). By 30 August (Figure 10) another large plume is obvious in the northern portion of the cross sections with large amounts of CO in the midtroposphere. Careful observation is required to view the continuing southward progression of the near surface CO feature between 32°N and 38°N. Examination of the AIRS CO maps in Figure 4 indicates that the TES track was just east of the axis of the largest CO enhancements in this plume as it moved south on 28 and 30 August.

[37] Again, the diagonals of the averaging kernels on 30 August (Figure 10, right) show there is more information

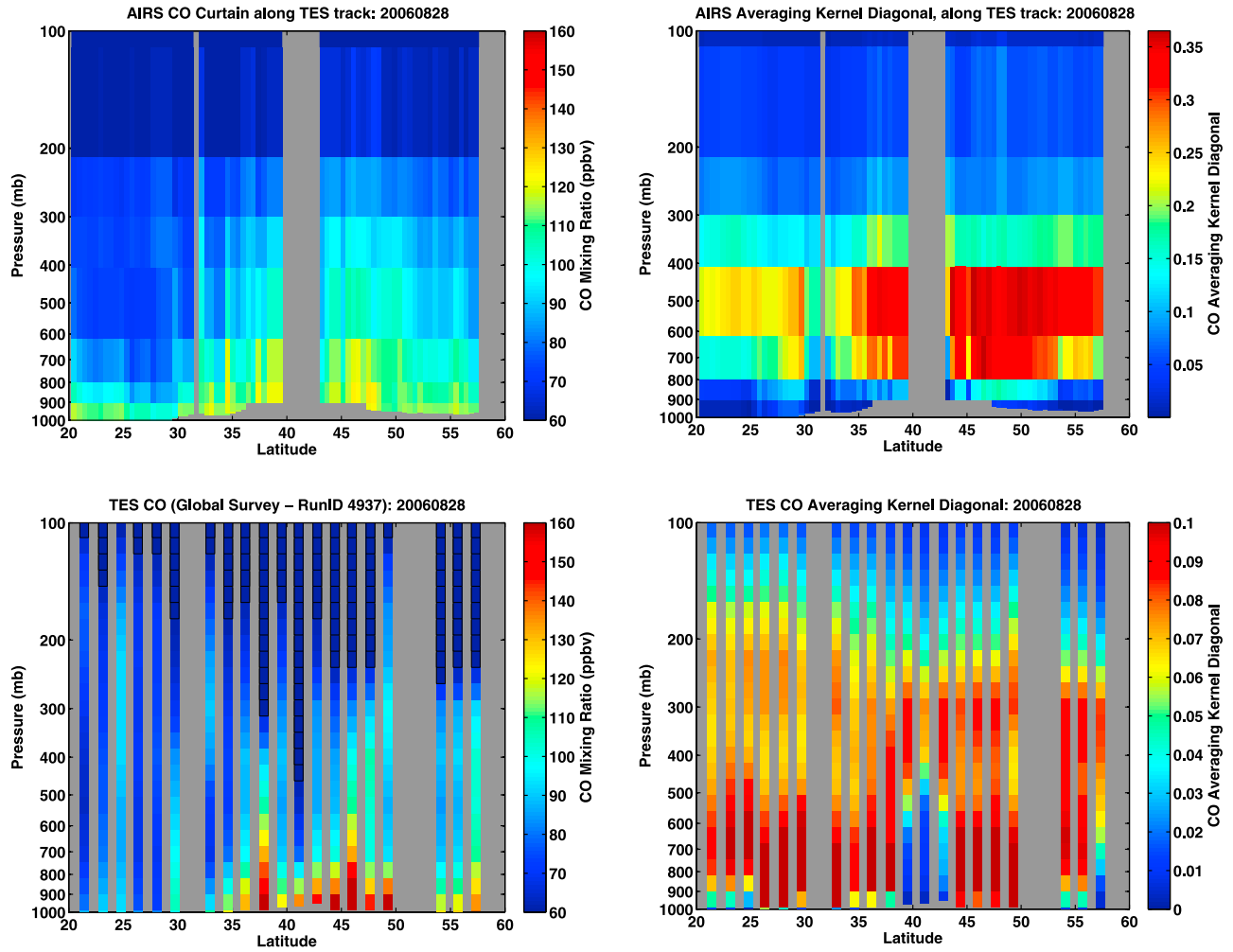

Figure 9. The 28 August global survey track: (top) AIRS and (bottom) TES cross sections of (left) retrieved CO and (right) diagonal of the CO averaging kernel. The location of these cross sections is noted in the AIRS CO and MODIS AOD maps of Figure 4.

near the surface over the Texas/Oklahoma CO enhancement than in regions of less enhancement. This change in sensitivity to the lower layers is illustrated further by comparing the averaging kernels for individual CO retrievals of AIRS and TES. Figure 11 presents the full averaging kernels for a retrieval in the region of CO enhancement (left) and to the north in cleaner air (right). The averaging kernels for the lowest three AIRS trapezoidal perturbation functions (heavy red lines) are larger below 700 mb in the enhanced CO region. In particular, the two lowest functions are nearly twice as large in the enhanced region than in the clean region. Thus, although the AIRS CO retrieval cannot fully resolve the enhanced CO in the lowest 2 km, the retrieval does respond to the enhancement. The TES averaging kernels also indicate a greater sensitivity to CO below 700 mb in the region of CO enhancement. Both AIRS and TES averaging kernels show they are rapidly losing sensitivity below 900 mb, and their surface retrievals will most likely be biased low. Ground-based in situ measurements of CO in Oklahoma and Texas provide supporting evidence for this lower tropospheric CO transport as discussed in the next section.

3.3. Ground-Based Observations

[38] As we discuss below, ground-based observations from the SGP site near Lamont, Oklahoma, the KWKT tower in Moody, Texas, and the Moody Tower dormitory at the University of Houston show the southward progression of a region of CO enhancement which mixed to the surface layer. Consistent with the MODIS AOD maps in Figure 4, aerosol scattering profiles from the Raman Lidar at the SGP site indicate this CO plume lacked significant aerosols from smoke. EPA speciated aerosol measurements across Oklahoma and Texas generally confirm this lack of smoke aerosols. However, speciated aerosol measurements from Houston and other coastal Texas sites exhibit an increase in organic carbon (OC) nearly coincident with the arrival of the CO plume.

3.3.1. Lamont, Oklahoma (ARM SGP)

[39] Figure 12 presents time series of CO, wind direction, wind speed, and sensible heat flux from a 60 m instrumented tower at the ARM SGP site near Lamont, Oklahoma. Plotted are 10 minute averages of CO mixing ratio and 30 minute averages of meteorological parameters. The CO time series (Figure 12a) illustrates two prominent increases

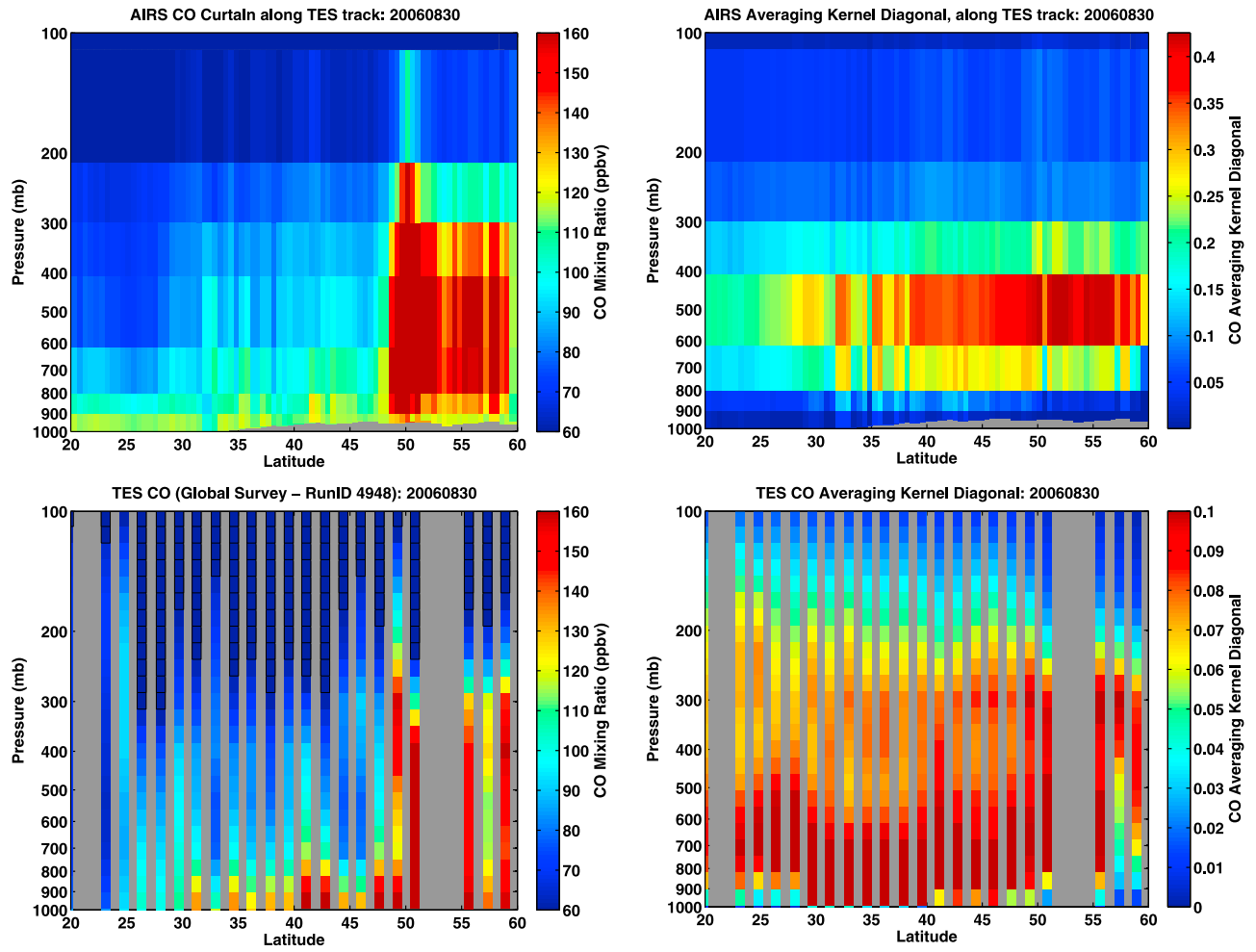

Figure 10. The 30 August global survey track: (top) AIRS and (bottom) TES cross sections of (left) retrieved CO and (right) diagonal of the CO averaging kernel. The location of these cross sections is noted in the AIRS CO and MODIS AOD maps of Figure 4.

on 28 August, the first between 0500 and 1000 UTC and the second centered around 1500 UTC. The second increase coincides with the change in wind direction (Figure 12b) from westerly to northerly in association with arrival of the cold front at the surface. The sensible heat flux (Figure 12d) indicates the CO peak nearly coincides with the first convective overturning of the day. Thus, we infer the CO was being mixed down from a plume aloft over the SGP, though there is some evidence the CO starts to increase slightly before the sensible heat.

[40] Careful examination of the sensible heat flux time series shows a small negative excursion preceding the first increase. This negative sensible heat flux coincides with a rapid change in the wind speed at 1400 UTC and the increase in CO. This change in wind speed marks the arrival of a burst of shear driven turbulent mixing in the shallow nocturnal boundary layer and is responsible for the initial mixing down of CO from a plume aloft [*Salmond and McKendry*, 2005]. Moreover, the first, more erratic period of CO increase between 0500 and 1000 UTC coincides with a number of small negative fluctuations in sensible heat and local maxima in the wind speed.

[41] Aerosol profiles retrieved from measurements made by the Raman Lidar at the SGP site [*Goldsmith et al.*, 1998; *Turner et al.*, 2002] on 28 and 29 August 2006 exhibit no aerosol plume coincident with the CO plume. Some tenuous aerosol features are present in the lowest 2 km but none with depolarization ratios consistent with smoke. It is possible that numerous clouds evident in the lidar profiles obscure the overhead smoke plume, or as the MODIS images suggest, perhaps there were few aerosols present with this portion of the CO plume. The subsequently discussed trajectory simulations indicate the Pueblo Fire parcels passed west of the SGP site. Unfortunately, the archived surface in situ aerosol measurements from the SGP site yielded no useful data for 28 and 29 August 2006.

3.3.2. KWKT TV Tower

[42] Figure 13 presents the time series of CO, wind direction, wind speed, and O_3 for 29 August from the KWKT TV tower in Moody, Texas. Each CO data point represents a 120 second average of data collected at 1 Hz. CO measurements (Figure 13a) are acquired alternately at three levels, 30, 122, and 457 m roughly every 15 minutes with all three levels exhibiting a large increase between 1600 and 1800 UTC. The CO increase propagates down with CO increasing first at 457 m (1639–1814 UTC), then 122 m (1654–1934 UTC), followed closely at 30 m (1704–1929 UTC). Passage of the cold front at KWKT coincides

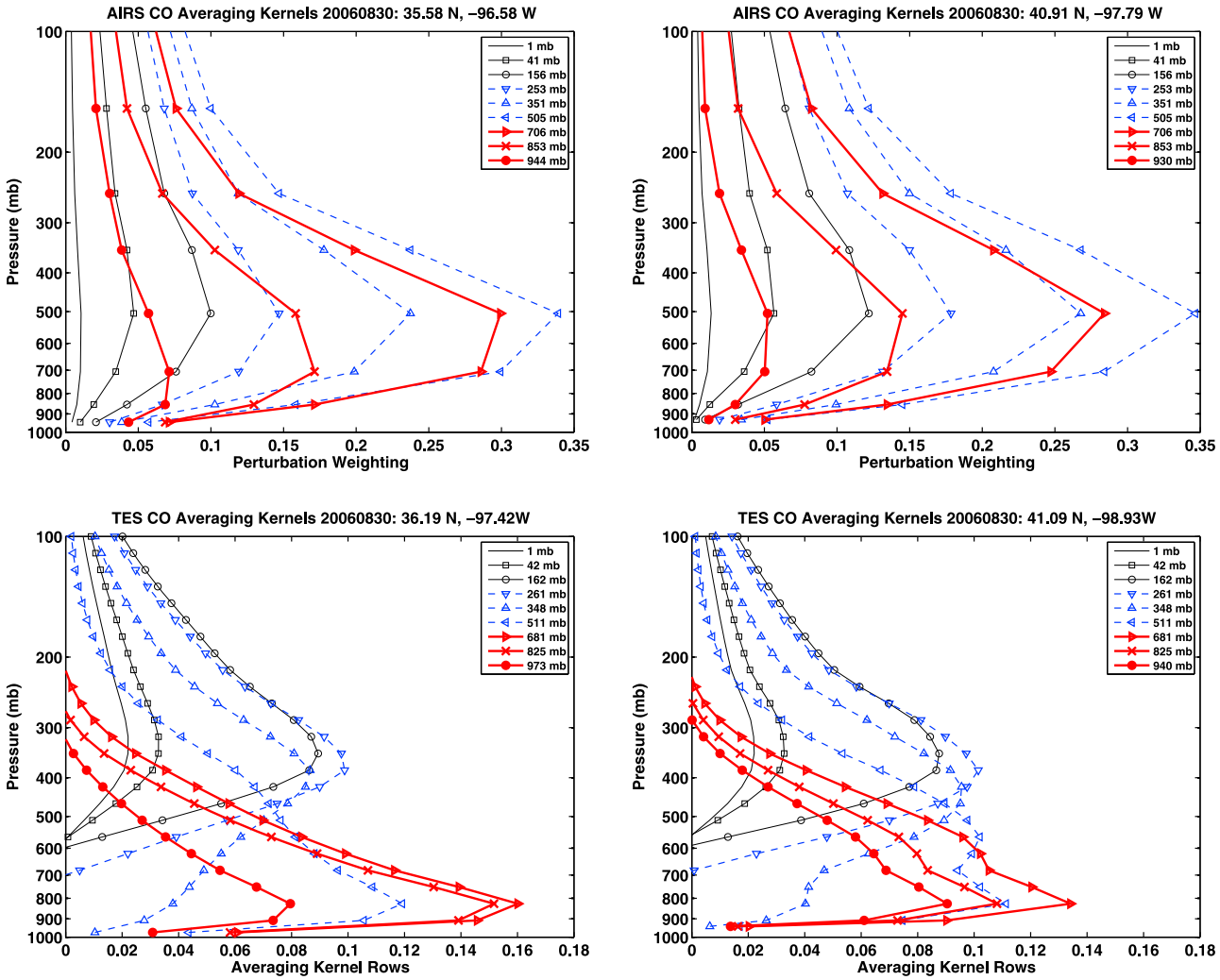

Figure 11. (top) AIRS CO averaging kernels and (bottom) TES CO averaging kernels from 30 August for (left) a CO enhancement over Texas and (right) a clean region over Nebraska.

with the CO increase on the 29th as noted by the change in wind direction (Figure 13b) from west-northwest to north-northeast. Note, the wind speed at 457 m shows a slight increase just before the shift in wind direction and at nearly the same time as the CO increase at that altitude. The 30 m wind exhibits a small increase approximately 30 minutes later near the time of the CO increase at that altitude and the wind direction shift. These wind speed increases could be indicative of turbulent mixing. Plotted are 10 minute average wind data computed from 30 second means.

[43] The O_3 time series [*Andrews et al.*, 2008] (Figure 13d) exhibits a diurnal cycle at 10 m but an interesting decoupling of the 457 m and 10 m layers between 0000 to 1700 UTC on 29 August followed by a sharp rise with the arrival of the cold front and thereafter. The decoupling can be interpreted as the result of a very thin nocturnal boundary layer overnight on 29 August [*Rappenglück et al.*, 2004; *Salmond and McKendry*, 2005]. The rapid increase at 457 m after 1700 UTC with abundances equal to that at 10 m indicates a well mixed region. However, the increase in CO and wind speeds at 457 m occur at least 30 minutes before the 457 m O_3 begins to increase, thus indicating the CO was mixed down from above and not carried up with the rising boundary layer. Some of this O_3 increase on 29 August could be attributed to influx of O_3 rich air along with the CO as well as increased local O_3 production, but these measurements alone are not conclusive.

3.3.3. Houston, Texas (UH Moody Tower)

[44] Figure 14 presents a time series of ten minute averaged CO, wind direction, wind speed, and O_3 from the University of Houston Moody Tower from 28 August through 2 September. The wind direction (Figure 14b) illustrates the transition from southerly to northerly flow from 28 to 29 August and the passage of the cold front late on 29 August with north to northeasterly flow on 30 August. Throughout this transition, background CO abundances (Figure 14a) increase from approximately 100 ppbv early on 28 August to nearly 200 ppbv early on 30 August (see also Lefer et al., submitted manuscript, 2009). The prominent twice daily peaks in CO on 28 and 29 August result from local rush hour vehicular traffic on Monday and Tuesday, respectively. These traffic peaks are less prominent on 30 August, but on 31 August, the morning peak reached 704 ppbv. An extremely shallow nocturnal boundary layer on the morning of 31 August [*Rappenglück et al.*, 2008] likely

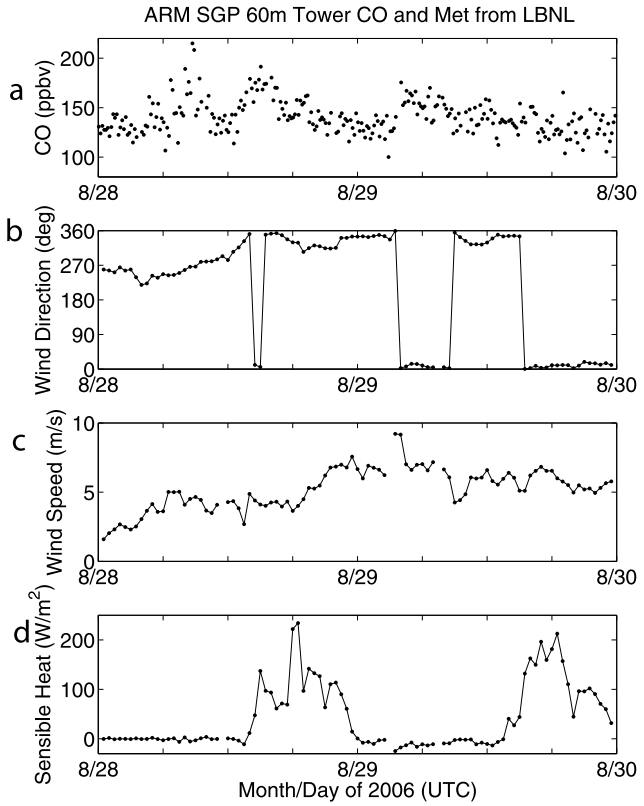

Figure 12. Time series of observations from the ARM SGP 60 m tower including (a) CO, (b) wind direction, (c) wind speed, and (d) sensible heat flux for 28 and 29 August 2006.

led to the large buildup of CO during this morning rush hour [*Rappenglück et al.*, 2004; *Salmond and McKendry*, 2005].

[45] The increase in background CO is consistent with the arrival of CO rich air transported behind the cold front from the fires which burned on 22–24 August in the Pacific Northwest. Further, the early morning CO peak of 675 ppbv

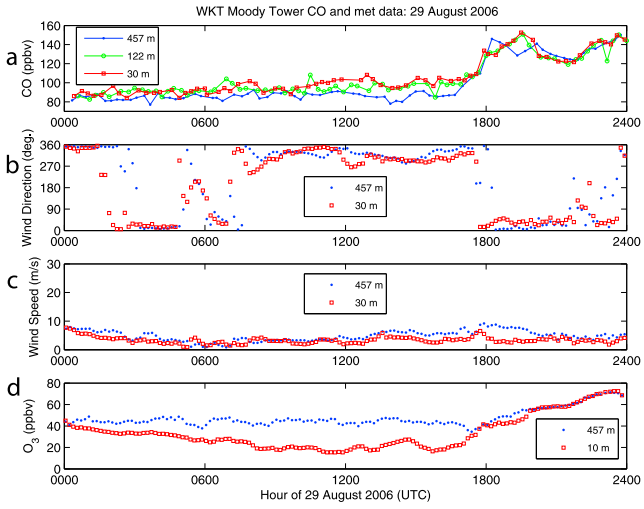

Figure 13. Time series of observations from the NOAA instrumented KWKT TV tall tower including (a) CO, (b) wind direction, (c) wind speed, and (d) O_3 on 29 August 2006.

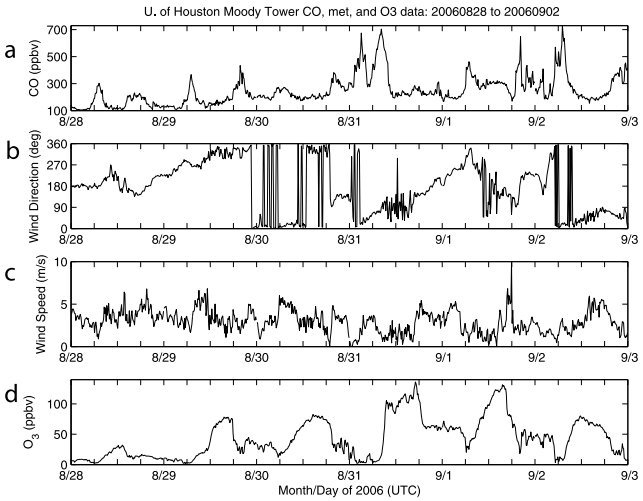

Figure 14. Time series of observations from the University of Houston Moody Tower dormitory including (a) CO, (b) wind direction, (c) wind speed, and (d) O_3 from 28 August through 2 September.

on 31 August at approximately 0300 UTC could have resulted from turbulent mix-down of an enhanced CO plume above the thin nocturnal boundary layer similar to that observed at the SGP site on 28 August. At approximately 0300 UTC on 31 August, the CO increases during a period of increasing wind speed, third panel, which is followed by a small increase in O_3 (Figure 14d). This small nocturnal increase in O_3 is a signature of mixing of air from above the nocturnal boundary layer [*Salmond and McKendry*, 2005]. *Morris et al.* [2010] found similar nocturnal mixing events occurred at another downtown Houston site during the nights of 30 and 31 August with O_3 mixing down from the residual layer into the surface layer.

[46] The Moody Tower O_3 time series exhibits an increasing diurnal variation from 28 August with 31 August lacking a significant depletion until just before sunrise on 1 September. The wind direction time series on 31 August indicates the dominance of the local sea breeze with winds rotating 360° through the day. As noted by *Rappenglück et al.* [2008] and Lefer et al. (submitted manuscript, 2009), northerly flow with a local sea breeze recirculation often leads to large values of surface O_3 in Houston. At Moody Tower, O_3 again was elevated on 1 September.

3.3.4. Houston Speciated Aerosols

[47] EPA speciated aerosol measurements for August and September 2006 were examined for evidence of smoke impacting the southern plains and Texas. Organic carbon (OC) increases occurred at several sites in Texas around the time of the frontal passage, but the coarse 3 day temporal sampling makes determination of precise timing impossible. The OC increase was most notable for the near coastal cities of Port Arthur, Houston, Corpus Christi, and Brownsville. Table 2 presents the measurements from the Deer Park EPA site in Houston, Texas. At Deer Park, OC increased an order of magnitude from 27 to 30 August. However, both the fine particles smaller than 2.5 microns in diameter (PM2.5) and Potassium ions (K^+), exhibit increases on 27 August before the cold front arrived, and measured K^+ was essentially null

Table 2. Speciated Aerosol Measurements From Deer Park, Texas, by Date[a]

Date	OC	K^+	$PM_{2.5}$	Sulfate
21 Aug 2006	0.76	0.02	9	3.38
24 Aug 2006	0.77	-	-	-
27 Aug 2006	0.44	0.06	20.5	2.34
30 Aug 2006	4.8	0	18.4	5.71
02 Sep 2006	4.84	0.07	19.2	6.49
05 Sep 2006	5.25	0.05	21.1	6.44
08 Sep 2006	3.91	0	27.9	10.4
11 Sep 2006	2.3	0.02	11.5	3.45

[a]Unit is $\mu g/m^3$. Only organic carbon (OC) measurements were made on 24 August.

on 30 August. The increase in sulfate aerosols on 30 August indicates a significant influence of anthropogenic sources. The other Houston area EPA speciation site (ID 422010024) saw a factor of 5 increase in OC and a doubling of K^+ and sulfate aerosols between 27 August and 2 September. OC increases in central Texas were smaller with similar small changes in K^+. With the number of industrial sources in the immediate Houston area as well as urban areas upwind under northerly flow (Dallas and farther away, Chicago), it is not surprising that a complex mix of aerosols would occur together during this air quality exceedance. However, due to the spread in timing and lack of signatures at other EPA sites in the southern plains, we cannot identify conclusively a source for any of these aerosols.

3.4. Trajectory and Model Simulations

[48] Figure 15 summarizes the results of the GKFTC forward trajectory simulations and the RAQMS model and confirms the CO plume transport seen by AIRS and the timing of CO plume arrival from the surface observations. Starting with the first row of maps, parcels initialized at 700 mb over the Pacific Northwest fires on 23 August (see Figure 5) move east and rise over the Rocky Mountains. Along the CALIPSO track on 24 August, noted on the map, the parcels to the north are at a higher altitude than those to the south agreeing with the aerosol plume seen by CALIPSO (Figure 7). The 24 August spatial pattern of RAQMS CO and BCOC match the trajectories, AIRS CO, and MODIS AOD maps (Figure 4) showing most of the fire emissions moved northeastward into Canada.

[49] Subsequently, both the trajectories and RAQMS maps show the higher altitude parcels stream across southern Canada while those at lower altitudes linger over the Northern Plains as they stretch as far east as Minnesota by 26 August. This eastward stretching is consistent with the AIRS CO retrievals for the same date but is not evident in MODIS AOD (Figure 4). The RAQMS BCOC contours indicate transport further to the east over the Great Lakes. Both the trajectories and RAQMS CO field show a subtle southward transport feature from southwestern Nebraska into the northwestern Texas panhandle.

[50] By 28 August, both the GKFTC trajectories and RAQMS fields find southward transport into Oklahoma. The trajectories indicate descent along the leading edge of parcels passing near the SGP site. Although RAQMS BCOC contours show enhancements in the vicinity of the SGP site, the bulk of the southward BCOC transport appears to the west in agreement with the GKFTC trajectories. Thus, the plume may have only brushed the SGP site with few aerosols for the Raman Lidar to see.

[51] The 30 August maps (Figure 15) reveal the plume has swept through central Texas all the way to Houston and the Louisiana Gulf Coast having passed the KWKT tower on 29 August (map not shown for brevity). The deepening red colors of the parcels as they move south denote descent with a number sticking to the surface in east central Texas on 31 August. The majority of these trajectories terminating at the surface originated from the Pueblo Fire. The north-northwest/south-southeast alignment of the parcels and RAQMS CO stretching from Texas to North Dakota closely resemble the CO distribution seen by AIRS on this date (Figure 4). The RAQMS BCOC enhancement in central Texas on the leading edge of the CO plume is consistent with the MODIS AOD retrievals showing a gradient roughly parallel to the TES track and some higher values in southern and eastern Texas (Figure 4). Detailed analysis of the trajectories indicate the bulk of the north-northwest/south-southeast alignment across central Texas on 31 August originated from the Columbia Complex Fire.

[52] A subset of parcels initialized over the Pueblo Fire are outlined in black on all trajectory maps (Figure 15). These Pueblo parcels move east to Minnesota on 26 August before turning south and crossing near Houston on 30 August. By 31 August, they have stretched into an arcuate feature over the northern Gulf of Mexico. This feature is remarkably similar to the arcuate aerosol feature visible in the MODIS AOD map for this date (Figure 4). Prior to 31 August, the motion of these parcels is consistent with the RAQMS BCOC contours and could have contributed to the organic carbon increase measured at the Deer Park and other EPA sites along the Texas coast on 30 August and 2 September. Although the depicted RAQMS BCOC contours show some transport to the Gulf Coast, the 700 mb level does not reproduce the Gulf of Mexico aerosol arc nor does model output at any other altitude. With this transport due to a frontal system, it is possible RAQMS overestimated some of the wet deposition or that it lacks the spatial resolution to capture this feature. However, the RAQMS CO distribution does produce an arcuate gradient across the Gulf of Mexico, blue to purple contour, nearly coincident with the trajectory arc. The location of this arc falls in a gap between orbits for AIRS CO data on this date (Figure 4).

[53] Examination of the 30 and 31 August 700 mb RAQMS CO distributions shows contributions to Gulf Coastal CO from both the fires in the Pacific Northwest (more to the west of Houston) and the heavily populated industrial region of the Great Lakes (more to the east of Houston). *Pierce et al.* [2009] detail the influence of the industrial Midwest on the continued O_3 exceedance from 1 to 4 September 2006.

[54] Here we have presented results from one GKFTC trajectory simulation initialized at 700 mb at 1800 UTC over the MODIS detected hot spots of 23 August using GFS winds. Similar transport patterns result for 700 and 850 mb trajectories starting from 1800 UTC on 22 August through 1800 UTC on 24 August, approximately the duration of the fire event illustrated in Figure 6. Earlier trajectories do not move south nor do later trajectories. Parcels initialized at higher altitudes move rapidly to the east. Thus, we believe the majority of the emissions that reached Texas from these

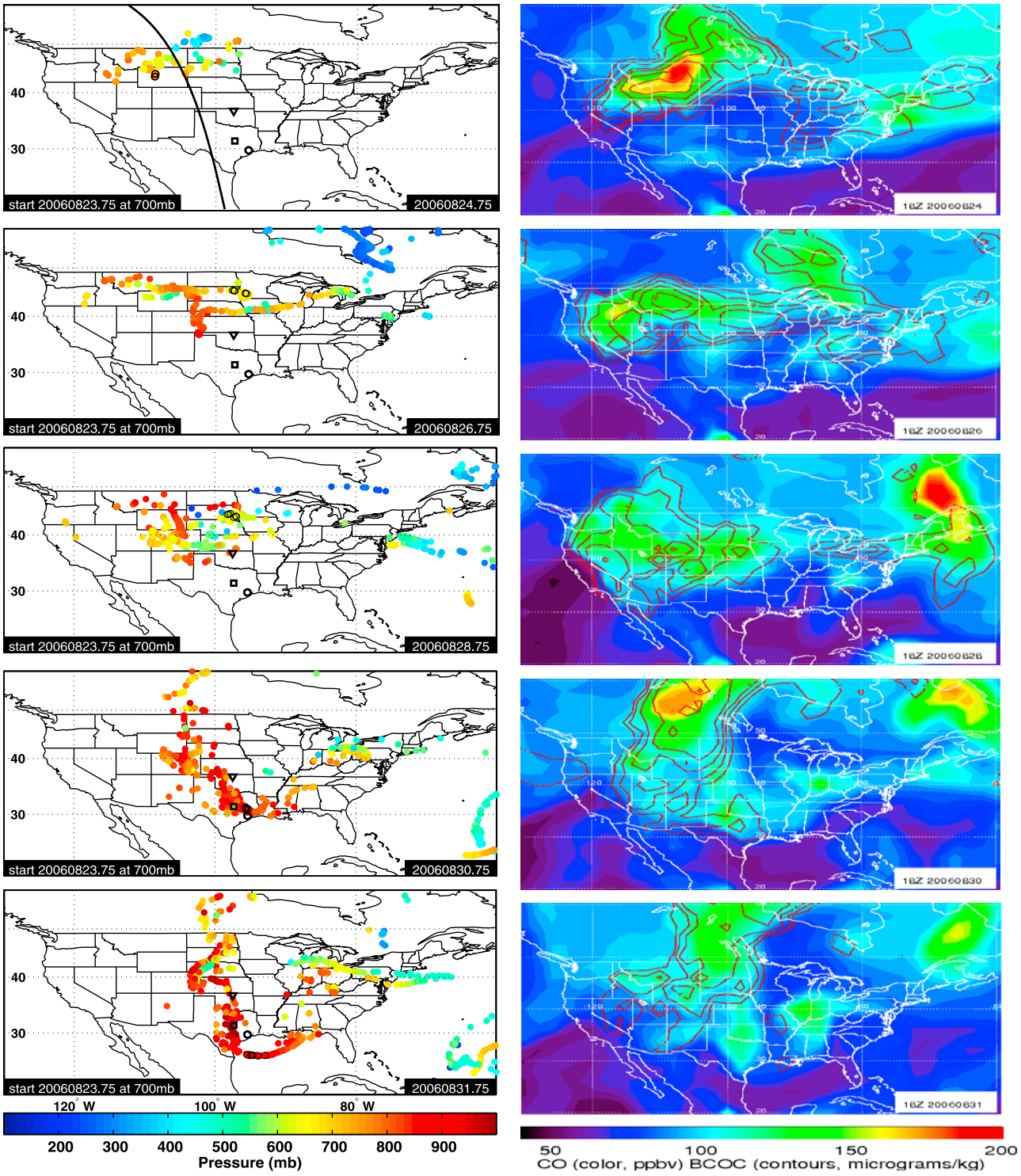

Figure 15. Forward trajectories from the (left) GKFTC model and (right) RAQMS 700 mb output for 1800 UTC on 24, 26, 28, 30, and 31 August 2006. Trajectory parcels were initialized at 700 mb and 1800 UTC on 23 August over the Figure 5 MODIS hot spots. RAQMS CO (color) and BCOC (red contours: 1, 2, 4, 8, 16, 32 μg/kg) are displayed. The 24 August CALIPSO cross section and locations of the ARM SGP site (triangle), WKT tower (square), and Houston (circle) are noted in the trajectory maps. A subset of parcels from the Pueblo Fire is outlined in black.

fires were injected no higher than approximately 700 mb. Contributions to the Houston area from fires burning elsewhere in the western United States (see Figure 5) were negligible during this time period. Although trajectories run using NCEP reanalysis winds at lower spatial resolution show similar overall transport patterns, they exhibit much less structure and are too slow when compared to the ground site observations. However, these NCEP

trajectories indicate transport from the later 28–30 August pulse in fire activity in the Pacific Northwest similarly influenced the Houston area into the first week of September as the prevailing northerly flow meandered from the north-northwest, to north-northeast, and back.

4. Conclusions

[55] Addressing one of the key goals of the 2006 Texas Air Quality Study, this analysis documents a case of distant pollution sources contributing to poor air quality in the greater Houston region. We have demonstrated the capability of AIRS observations to track the daily motion of CO from source to receptor: from fires in the Pacific Northwest to O_3 production in Houston, Texas. Pushing AIRS CO retrievals to their limits of monitoring CO transport in the lowest 3 km of the troposphere, we confirm this transport using a combination of TES CO cross sections, surface in situ CO measurements, and model simulations.

[56] RAQMS black and organic carbon distributions find some transport from the fires to the Houston area, but MODIS AOD, ground-based Raman Lidar, and surface speciated aerosol observations indicate much of the smoke aerosols may have been removed prior to the southward movement of the CO plume. However, CALIPSO aerosol profiles close to the fires are key to determining the smoke injection height from the fires. This height is confirmed by the motion of CO as seen by AIRS and illustrated by forward trajectory simulations and results of the RAQMS model. The forward trajectory simulations suggest an arcuate feature consistent with the MODIS observed aerosol arc over the northern Gulf of Mexico originated in emissions from the Pueblo Fire in southeastern Oregon. However, the lack of a similar feature in the RAQMS black carbon and organic carbon distributions points to the complexity of precisely modeling the long range transport of such fire emissions.

[57] The forward trajectory and RAQMS results also match the timing of the CO increases observed at the ARM SGP site in north central Oklahoma, the KWKT tall tower and the University of Houston Moody Tower dormitory. Careful examination of nighttime measurements from both the SGP site and Moody Tower indicate the influence of turbulent mixing in the shallow nocturnal boundary layer for bringing enhanced CO in the aloft plume down to the surface. During the subsequent morning, the presence of increased CO near the surface contributed to increased O_3 production. Close examination of the forward trajectory simulations indicate the two largest fires burning in the Pacific Northwest in the last week of August 2008 had the greatest impact on CO in Texas: the Pueblo Fire in southeastern Oregon and the Columbia Complex Fire in southeast Washington.

[58] In the last two years, the daily observations from AIRS have been augmented by the Infrared Atmospheric Sounding Interferometer (IASI) onboard the European METOP-A satellite. IASI's morning orbit affords more complete diurnal coverage than AIRS alone and is the first of three instruments planned to fly over the next 15 years. Moreover, IASI's superior spectral resolution provides more vertical information in CO retrievals, particularly near the surface over land during the daytime [*George et al.*, 2009]. Future NASA satellite missions focused on air quality may pave the way for routine observations of chemical weather much as current geostationary observations contribute to the current numerical weather forecasts.

[59] **Acknowledgments.** We were deeply saddened by the passing of coauthor Chieko Kittaka during the initial review of this manuscript. Her inputs to the revisions were sorely missed. The authors gratefully acknowledge support from the NASA EOS Program through NASA grants NAG5-11163, NAG5-11653, NNG04GN42G, and NNG06GB06G. Our thanks go to Minnie Wong at the University of Maryland, Fire Information for Resource Management System and the MODIS Rapid Response Project, for providing the MODIS hot spot data. The tower measurements in Oklahoma were supported by the U.S. Department of Energy, Office of Science, Division of Biological and Environmental Research, Atmospheric Radiation Measurement Program, under contract DE-AC03-76SF00098. Analysis of the Raman lidar data was partially supported by DOE grant DE-FG02-08ER64538 to the University of Wisconsin-Madison. We thank Mark Schoeberl for access to the GSFC trajectory code. Thanks go to the entire AIRS Team, particularly our NOAA collaborators Chris Barnet and Walter Wolf, and the personnel at NASA DISC. A special note of thanks goes to Bruce Doddridge of NASA and Fred Fehsenfeld of NOAA for supporting our involvement with TexAQS II. The views, opinions, and findings contained in this report are those of the author(s) and should not be construed as an official National Oceanic and Atmospheric Administration or U.S. Government position, policy, or decision. W.W.M. thanks Rae Force for her unwavering support.

References

AIRS Project Office (2007a), AIRS/AMSU/HSB version 5 Level 2 quality control and error estimation, version 1.0, report, Jet Propul. Lab., Pasadena, Calif.

AIRS Project Office (2007b), AIRS version 5 release Level 2 standard product quickstart, version 1.0, report, Jet Propul. Lab., Pasadena, Calif.

American Lung Association (2008), American Lung Association state of the air 2008, report, New York.

Andrews, A., et al. (2008), Tall-tower observations of pollution from near-field sources in central Texas during the Texas Air Quality Study 2006, *Eos Trans. AGU*, *89*(53), Fall Meet. Suppl., Abstract A33B-0237.

Badr, O., and S. D. Probert (1994), Carbon monoxide concentration in the Earth's atmosphere, *Appl. Energy*, *49*, 99–143.

Bakwin, P. S., P. P. Tans, D. F. Hurst, and C. Zhao (1998), Measurements of carbon dioxide on very tall towers: Results of the NOAA/CMDL program, *Tellus, Ser. B.*, *50*, 401–415.

Beer, R. (2006), TES on the Aura mission: Scientific objectives, measurements and analysis overview, *IEEE Trans. Geosci. Remote Sens.*, *44*, 1102–1105.

Chu, D. A., Y. J. Kaufman, G. Zibordi, J. D. Chern, J. M. Mao, C. Li, and H. B. Holben (2003), Global monitoring of air pollution over land from Earth Observing System–Terra MODIS, *J. Geophys. Res.*, *108*(D21), 4661, doi:10.1029/2002JD003179.

Colarco, P., M. R. Schoeberl, B. G. Doddridge, L. T. Marufu, O. Torres, and E. J. Welton (2004), Transport of smoke from Canadian forest fires to the surface near Washington, D.C.: Injection height, entrainment, and optical properties, *J. Geophys. Res.*, *109*, D06203, doi:10.1029/2003JD004248.

Crutzen, P. J., L. E. Heidt, J. P. Krasnec, and W. H. Pollock (1979), Biomass burning as a source of atmospheric gases CO, H_2, N_2O, NO, CH_3Cl and COS, *Nature*, *282*, 253–256.

Darby, L. (2005), Cluster analysis of surface winds in Houston, Texas, and the impact of wind patterns on ozone, *J. Appl. Meteorol.*, *44*, 1788–1806.

Daum, P. H., L. I. Kleinman, S. R. Springston, L. J. Nunnermacker, Y. N. Lee, J. Weinstein-Lloyd, J. Zheng, and C. Berkowitz (2004), Origin and properties of plumes of high ozone observed during Texas 2000 Air Quality Study (TexAQS 2000), *J. Geophys. Res.*, *109*, D17306, doi:10.1029/2003JD004311.

Davis, J. M., B. K. Eder, D. Nychka, and Q. Yang (1998), Modeling the effects of meteorology on ozone in Houston using cluster analysis and generalized additive models, *Atmos. Environ.*, *32*, 755–781.

Fischer, M. L., D. P. Billesbach, W. Riley, J. A. Berry, and M. S. Torn (2007), Spatiotemporal variations in growing season exchanges of CO_2, H_2O, and sensible heat in agricultural fields of the southern great plains, *Earth Interact.*, *11*(17), 1–21.

Forster, C., et al. (2001), Transport of boreal forest fire emissions from Canada to Europe, *J. Geophys. Res.*, *106*(D19), 22,887–22,906.

George, M., et al. (2009), Carbon monoxide distributions from the IASA/METOP mission: Evaluation with other spaceborne remote sensors, *Atmos. Chem. Phys.*, *9*, 8317–8330.

Giglio, L., J. Descloitres, C. Justice, and Y. Kaufman (2003), An enhanced contextual fire detection algorithm for modis, *Remote Sens. Environ.*, *87*, 273–282.

Goldsmith, J. E. M., F. H. Blair, S. E. Bisson, and D. D. Turner (1998), Turn-key Raman lidar for profiling atmospheric water vapor, clouds, and aerosols, *Appl. Opt.*, *37*, 4979–4990.

Kahn, R. A., Y. Chen, D. L. Nelson, F. Y. Leung, Q. Li, D. J. Diner, and J. A. Logan (2008), Wildfire smoke injection heights: Two perspectives from space, *Geophys. Res. Lett.*, *35*, L04809, doi:10.1029/2007GL032165.

Kaufman, Y. J., L. A. Tanre, D. Remer, E. Vermote, D. A. Chu, and B. N. Holben (1997), Operational remote sensing of tropospheric aerosol over land from EOS moderate resolution imaging spectroradiometer, *J. Geophys. Res.*, *102*(D14), 17,051–17,067.

Kleinman, L., P. Daum, D. Imre, Y. Lee, L. Nunnermacker, S. Springston, J. Weinstein-Lloyd, and J. Rudolph (2002), Ozone production rate and hydrocarbon reactivity in 5 urban areas: A cause of high ozone concentration in Houston, *Geophys. Res. Lett.*, *29*(10), 1467, doi:10.1029/2001GL014569.

Labonne, M., F. M. Bréon, and F. Chevallier (2007), Injection height of biomass burning aerosols as seen from a spaceborne lidar, *Geophys. Res. Lett.*, *34*, L11806, doi:10.1029/2007GL029311.

Levy, R. C., L. A. Remer, S. Mattoo, E. F. Vermote, and Y. J. Kaufman (2007), Second-generation algorithm for retrieving aerosol properties over land from MODIS spectral reflectance, *J. Geophys. Res.*, *112*, D13211, doi:10.1029/2006JD007811.

Logan, J. A., M. J. Prather, S. C. Wofsy, and M. B. McElroy (1981), Tropospheric chemistry: A global perspective, *J. Geophys. Res.*, *86*(C8), 7210–7254.

Luo, M., et al. (2007), TES carbon monoxide validation with DACOM aircraft measurements during INTEX-B 2006, *J. Geophys. Res.*, *112*, D24S48, doi:10.1029/2007JD008803.

McMillan, W. W., K. Evans, L. Yurganov, C. Wilson, G. Sachse, G. Diskin, C. Barnet, and E. Maddy (2008a), Validation of AIRS CO retrievals for air quality and transport assessments, *Eos Trans. AGU*, *89*(23), Joint Assem. Suppl., Abstract A33A-12.

McMillan, W. W., et al. (2008b), AIRS views of transport from 12 to 22 July 2004 Alaskan/Canadian fires: Correlation of AIRS CO and MODIS AOD with forward trajectories and comparison of AIRS CO retrievals with DC-8 in situ measurements during INTEX-A/ICARTT, *J. Geophys. Res.*, *113*, D20301, doi:10.1029/2007JD009711.

Morris, G., et al. (2006), Alaskan and Candian forest fires exacerbate ozone pollution over Houston, Texas on 19 and 20 July 2004, *J. Geophys. Res.*, *111*, D24S03, doi:10.1029/2006JD007090.

Morris, G., B. Ford, B. Rappenglück, A. M. Thompson, A. Mefferd, F. Ngan, and B. Lefer (2010), An evaluation of the influence of the morning residual layer on afternoon ozone concentrations in Houston using ozonesonde data, *Atmos. Environ.*, doi:10.1016/j.atmosenv.2009.06.057, in press.

Naranjo, L. (2008), Regional pollution goes local, in *Sensing Our Planet: NASA Earth Science Research Features 2008*, edited by J. Bietler, pp. 20–23, NASA, Greenbelt, Md.

Novelli, P. C., K. A. Masarie, P. M. Lang, B. A. Hall, and R. C. Myers (2003), Reanalysis of tropospheric CO trends: Effects of the 1997–1998 wildfires, *J. Geophys. Res.*, *108*(D15), 4464, doi:10.1029/2002JD003031.

Pierce, R. B., et al. (2007), Chemical data assimilation estimates of continental U.S. ozone and nitrogen budgets during the Intercontinental Chemical Transport Experiment–North America, *J. Geophys. Res.*, *112*, D12S21, doi:10.1029/2006JD007722.

Pierce, R. B., et al. (2009), Impacts of background ozone production on Houston and Dallas, TX air quality during the TexAQS field mission, *J. Geophys. Res.*, *114*, D00F09, doi:10.1029/2008JD011337.

Potosnak, M. J., S. C. Wofsy, A. S. Denning, T. J. Conway, J. W. Munger, and D. H. Barnes (1999), Influence of biotic exchange and combustion sources on atmospheric CO_2 concentrations in New England from observations at a forest flux tower, *J. Geophys. Res.*, *104*(D8), 9561–9569.

Rappenglück, B., C. Forster, G. Jakobi, and M. Pesch (2004), Unusually high levels of PAN and ozone over Berlin, Germany, during nighttime on August 7, 1998, *Atmos. Environ.*, *38*, 6125–6134.

Rappenglück, B., R. Perna, S. Zhong, and G. A. Morris (2008), An analysis of the vertical structure of the atmosphere and the upper-level meteorology and their impact on surface ozone levels in Houston, Texas, *J. Geophys. Res.*, *113*, D17315, doi:10.1029/2007JD009745.

Remer, L. A., et al. (2005), The MODIS aerosol algorithm, products and validation, *J. Atmos. Sci.*, *62*, 947–973.

Ryerson, T., et al. (2003), Effect of petrochemical industrial emissions of reactive alkenes and NO_x on tropospheric ozone formation in Houston, Texas, *J. Geophys. Res.*, *108*(D8), 4249, doi:10.1029/2002JD003070.

Salmond, J. A., and I. G. McKendry (2005), A review of turbulence in the very stable nocturnal boundary layer and its implications for air quality, *Prog. Phys. Geogr.*, *29*(2), 171–188, doi:10.1191/0309133305pp442ra.

Schoeberl, M., and L. Sparling (1995), Trajectory modeling, in *Diagnostic Tools in Atmospheric Physics: Proceedings of the International School of Physics*, edited by G. Fiocco and G. Visconti, pp. 289–306, IOS Press, Amsterdam.

Schroeder, W., E. Prins, L. Giglio, I. Csiszar, C. Schmidt, J. Morisette, and D. Morton (2008), Validation of GOES and MODIS active fire detection products using ASTER and ETM+ data, *Remote Sens. Environ.*, *112*, 2711–2726.

Stohl, A., C. Forster, H. Huntrieser, W. McMillan, A. Petzold, H. Schlager, and B. Weinzierl (2007a), Aircraft measurements over Europe of an air pollution plume from Southeast Asia aerosal and chemical characterization, *Atmos. Chem. Phys.*, *7*, 913–937.

Stohl, A., et al. (2007b), Arctic smoke record air pollution levels in the European Arctic during a period of abnormal warmth, due to agricultural fires in Eastern Europe, *Atmos. Chem. Phys.*, *7*, 511–534.

Sunita, V., J. Worden, R. B. Pierce, D. Jones, J. A. Al-Saadi, K. Bowman, and F. Boersma (2009), Ozone production in boreal fire smoke plumes using observations from the Tropospheric Emission Spectrometer and the Ozone Monitoring Instrument, *J. Geophys. Res.*, *114*, D02303, doi:10.1029/2008JD010108.

Susskind, J., C. D. Barnet, and J. M. Blaisdell (2003), Retrieval of atmospheric and surface parameters from AIRS/AMSU/HSB data in the presence of clouds, *IEEE Trans. Geosci. Remote Sens.*, *41*, 390–409.

Susskind, J., J. M. Blaisdell, L. Iredell, and F. Keita (2010), Improved temperature sounding and quality control methodology using AIRS/AMSU data: The AIRS science team version 5 retrieval algorithm, *IEEE Trans. Geosci. Remote Sens.*, in press.

Thompson, A., et al. (2007), Intercontinental Chemical Transport Experiment Ozonesonde Network Study (IONS) 2004: 2. Tropospheric ozone budgets and variability over northeastern North America, *J. Geophys. Res.*, *112*, D12S13, doi:10.1029/2006JD007670.

Thompson, A., J. E. Yorks, S. K. Miller, J. C. Witte, K. M. Dougherty, G. A. Morris, D. Baumgardner, L. Ladino, and B. Rappenglück (2008), Free tropospheric ozone sources and wave activity over Mexico City and Houston during MILAGRO/Intercontinental Transport Experiment (INTEX-B) ozonesone network study 2006 (IONS-06), *Atmos. Chem. Phys.*, *8*, 5113–5125.

Turner, D. D., R. A. Ferrare, L. A. Heilman, L. A. Brasseur, W. F. Feltz, and T. P. Tooman (2002), Automated retrievals of water vapor and aerosol profiles from an operational Raman lidar, *J. Atmos. Oceanic Technol.*, *19*, 37–50.

Winker, D. M., W. H. Hunt, and M. J. McGill (2007), Initial performance assessment of CALIOP, *Geophys. Res. Lett.*, *34*, L19803, doi:10.1029/2007GL030135.

Yurganov, L. N., W. W. McMillan, A. Dzhola, E. Grechko, N. Jones, and G. van der Werf (2008), Global AIRS and MOPITT CO measurements, validation, comparison, and links to biomass burning variations and Carbon Cycle, *J. Geophys. Res.*, *113*, D09301, doi:10.1029/2007JD009229.

Zhang, L., et al. (2008), Transpacific transport of ozone pollution and the effect of recent Asian emission increases on air quality in North America: An intergrated analysis using satellite, aircraft, ozonesonde, and surface observations, *Atmos. Chem. Phys. Discuss.*, *8*, 8143–8191.

Zhao, C., P. S. Bakwin, and P. P. Tans (1997), A design for unattended monitoring of trace gases on a tall tower, *J. Atmos. Oceanic Technol.*, *14*, 1139–1145.

A. Andrews and S. Oltmans, Earth System Research Laboratory, NOAA, 325 Broadway, R/GMD 1, Boulder, CO 80305, USA.

S. Biraud and M. L. Fischer, Lawrence Berkeley National Laboratory, Berkeley, CA 94720, USA.

K. Evans and K. McCann, Joint Center for Earth Systems Technology, University of Maryland Baltimore County, 1000 Hilltop Cir., Baltimore, MD 21250, USA.

B. Lefer and B. Rappenglück, Department of Earth and Atmospheric Sciences, University of Houston, 4800 Calhoun Rd., Houston, TX 77204-5007, USA.

W. W. McMillan and L. C. Sparling, Department of Physics, University of Maryland Baltimore County, 1000 Hilltop Cir., Baltimore, MD 21250, USA. (mcmillan@umbc.edu)

R. Newsom, Pacific Northwest National Laboratory, Richland, WA 99352, USA.

G. Osterman, Jet Propulsion Laboratory, California Institute of Technology, Pasadena, CA 91109, USA.

R. B. Pierce, Cooperative Institute for Meteorological Satellite Studies, STAR, NESDIS, NOAA, University of Wisconsin-Madison, Madison, WI 53706, USA.

D. Turner, Space Science and Engineering Center, University of Wisconsin-Madison, Madison, WI 53706, USA.